Hygroscopic behavior of aerosols generated from solutions of 3-methyl-1,2,3-butanetricarboxylic acid, its sodium salts, and its mixtures with NaCl

Li Wu[1], Clara Becote[2,3,4], Sophie Sobanska[2], Pierre-Marie Flaud[3,4], Emilie Perraudin[3,4], Eric Villenave[3,4], Young-Chul Song[1], Chul-Un Ro[1*]

[1]Department of Chemistry, Inha University, Incheon, South Korea

[2]Institut des Sciences Moléculaires, UMR CNRS 5255, University of Bordeaux, Talence, France

[3]University of Bordeaux, EPOC, UMR 5805, 33405 Talence cedex, France

[4]CNRS, EPOC, UMR 5805, 33405 Talence cedex, France

Abstract

MBTCA (3-methyl-1,2,3-butanetricarboxylic acid), a low volatile, highly oxidized, secondary generation product of monoterpenes, is one of the most relevant tracer compounds for biogenic SOAs. In this study, laboratory-generated, micrometer-sized, pure MBTCA, mono-/di-/tri-sodium MBTCA salts, and MBTCA-NaCl mixture aerosol particles of four mixing ratios (molar ratios = 1:1, 1:2, 1:3, and 2:1) were examined systematically to observe their hygroscopic behavior by varying the relative humidity (RH) using in-situ Raman microspectrometry (RMS) assembled with either a see-through impactor where the particles were deposited on a Si wafer or a levitation system. The pure MBTCA droplets effloresced at RH = ~30-57.8% and did not deliquesce until RH > 95%. The mono- and di-sodium MBTCA salt aerosols did not show clear efflorescence RH (ERH) and deliquescence RH (DRH). In contrast, the tri-sodium MBTCA salt exhibited ERH = ~44.4-46.8% and DRH = ~53.1%, during the hygroscopic experiment cycle. The mixture aerosols generated from solutions of MBTCA:NaCl = 1:1 and 2:1 showed no visible ERH and DRH in the see-through impactor because of the partial and total consumption of NaCl, respectively, through chemical reactions during the dehydration process. The mixture particles with a 1:1 molar ratio in the levitation system exhibited a clear DRH at ~71% and ERH at ~50%. This suggests less reaction between the mixtures and a larger portion of NaCl remaining in the levitation system. The other

*Corresponding author. Tel.: +82 32 860 7676; Fax: +82 32 867 5604; E-mail: curo@inha.ac.kr

mixtures of MBTCA:NaCl = 1:2 and 1:3 displayed single-stage efflorescence and deliquescence at ERH = ~45-50% and DRH = ~74%, respectively, because of the considerable amount of NaCl present in the mixture aerosols in both systems. Observations and Raman analyses indicated that only monosodium MBTCA salt aerosols could be formed through a reaction between MBTCA and NaCl. The reaction occurred more rapidly with a more elevated concentration of either MBTCA or NaCl, and the controlling factor for the reactivity of the mixtures depended mostly on the availability of H^+ dissociated from the MBTCA tricarboxylic acid. The lower degree of reaction of the mixture particles in the levitation system might be caused by the relatively airtight circumstance inside, i.e., the less release of HCl. The study revealed that the interactions between the MBTCA and NaCl could modify the properties of the organic acid in the atmosphere, leading to enhanced capability of the probable heterogeneous chemistry in the aqueous aerosols.

1. Introduction

Chemical processes, such as gas-phase oxidations of airborne biogenic and anthropogenic volatile organic compounds (VOCs) by ozone (O_3), hydroxyl radical (OH), and nitrate radical (NO_3), and their condensed-phase reactions with preexisting aerosols, can promote the formation of increasingly oxidized and less volatile secondary organic aerosols (SOAs). SOAs are a ubiquitous and dominant fraction of the fine aerosol mass that exists as liquid, amorphous solid, semi-solid, and phase-separated aerosol particles (Jang et al., 2002; Hallquist et al., 2009; Jimenez et al., 2009; Virtanen et al., 2010; Koop et al., 2011; Bateman et al., 2015b; Shrivastava et al., 2015; Bernard et al., 2016; Pajunoja et al., 2016; Freedman, 2017; Shrivastava et al., 2017; Kim et al., 2018; Srivastava et al., 2018; Liu et al., 2019; Slade et al., 2019; Song et al., 2019; Wu et al., 2019a). These aerosols are of critical importance because of their ability to scatter and absorb solar radiation directly, to affect the number of CCN (cloud condensation nuclei) through the formation of new particles and the growth of preexisting particles, and further impact the climate and human health (Haywood and Boucher, 2000; Topping et al., 2013; Poschl and Shiraiwa, 2015; Reid et al., 2018; Marsh et al., 2019). SOAs are highly dynamic, multiphase chemical systems with a range of volatility and solubility and model simulations have claimed that the phase state of SOAs differs

according to the global locations and altitudes with an evolving relative humidity (RH), temperature, and particle composition (Kroll and Seinfeld, 2008; Shiraiwa et al., 2017).

Oxidative products of biogenic VOCs, such as monoterpenes (e.g., α- and β-pinenes), act as a dominant source of SOAs as they have high emission rates on a global scale and give considerable SOA yields, and they play a central role in new particle formation (Guenther et al., 1995; Lignell et al., 2013; Mutzel et al., 2016; Holopainen et al., 2017). Carboxylic acid-containing organic compounds comprise a large fraction of SOAs in the Northern Hemisphere (Yatavelli et al., 2015). An extremely low-volatile tricarboxylic acid, 3-methyl-1,2,3-butanetricarboxylic acid (MBTCA, $C_8H_{12}O_6$), has become one of the most relevant tracer compound for terpene SOAs (Jaoui et al., 2005; Szmigielski et al., 2007; Zhang et al., 2010; Donahue et al., 2012; Müller et al., 2012; Lai et al., 2015; Sato et al., 2016). In addition, it is also a few well-known compounds with a high O:C ratio that is formed in the oxidation of VOCs (Dunne et al., 2016). MBTCA is a second or later generation reaction product from monoterpenes by the OH-initiated oxidation of pinonic acid (PA) in the gaseous and aqueous phases and even at the air-water interface (Müller et al., 2012; Praplan et al., 2012; Aljawhary et al., 2016; Enami and Sakamoto, 2016). The MBTCA concentrations were found to be positively correlated with temperature because of the enhanced photochemical production of PA by OH radicals with increasing temperature (Hu et al., 2008; Zhang et al., 2010; Gómez-González et al., 2012; Miyazaki et al., 2012). A further reaction between MBTCA and OH radicals can result in CO_2 loss (Kostenidou et al., 2018). MBTCA was first observed at the Amazon basin and in summer aerosols from Ghent, Belgium (Kubátová et al., 2000; Kubátová et al., 2002). The compound was later found in the USA (Jaoui et al., 2005), Europe (Fu et al., 2009; Kourtchev et al., 2009; Zhang et al., 2010; Yasmeen et al., 2011; Gómez-González et al., 2012; Vogel et al., 2013; Kammer et al., 2018; Vlachou et al., 2019), Japan (Miyazaki et al., 2012), the polar regions (Hu et al., 2013), China (Hu et al., 2008; Ding et al., 2012; Li et al., 2013; Fu et al., 2014; Kang et al., 2018; Hong et al., 2019), and Australia (Cui et al., 2019). In addition, it has been observed in forest, marine, mountainous, urban, and rural aerosols, with its levels ranging from 0.03 to 100 ng/m^3, and the level was generally higher in the fine particle fraction than in the coarse fraction (Zhang et al., 2010).

The ability of the aerosol particles to uptake water in the air is dependent on one of the most important physicochemical properties, i.e., the hygroscopicity (Jimenez et al., 2009; Chu et al., 2014; Tang et al.,

2019; Wu and Ro, 2020). Hygroscopicity can help better understand the (i) aerodynamic properties, (ii) cloud-droplet nucleation efficiency, (iii) optical properties, and (iv) physicochemical changes through complicated heterogeneous chemical reactions of aerosol particles with various atmospheric gas-phase species. MBTCA was predicted to partition significantly into aerosol-liquid-water (ALW) (Aljawhary et al., 2016). Therefore, a study on the hygroscopic behavior of MBTCA is important for understanding its phase states better when it interacts with water vapor at different RHs as well as its impacts on the heterogeneous chemical reactions, atmospheric environment, and human health (Parsons et al., 2004; Mikhailov et al., 2009; Bateman et al., 2015a; Freedman, 2017; Slade et al., 2019). Atmospheric particles typically involve complex internal mixtures of organic and inorganic compounds (Shrivastava et al., 2017; Karadima et al., 2019). The interactions between organic and inorganic compounds may alter the chemical compositions of SOAs, which in turn affect their physicochemical properties, such as hygroscopicity (Rudich et al., 2007; Wu et al., 2011; Wang et al., 2015; Jing et al., 2016; Wang et al., 2018). Dicarboxylic acids (DCAs) can undergo reactions with inorganics, such as NaCl, resulting in Cl depletion and HCl liberation (Ma et al., 2013; Li et al., 2017). On the other hand, the interactions between tricarboxylic acids and inorganics have never been investigated.

In this study, in situ Raman microspectrometry (RMS) was used to examine the hygroscopic behavior, evolution of the chemical composition, phase states, and microstructures, and chemical reactivity of laboratory-generated, micrometer-sized aerosols generated from a pure MBTCA solution, mono-/di-/tri-sodium MBTCA salt solutions, and MBTCA-NaCl mixture solutions. RMS was assembled with either a see-through impactor, where the particles were deposited on a Si wafer, or a levitation system. The particles on the Si wafer were exposed to a hygroscopic measurement cycle, where they experienced a dehydration process first (by decreasing RH from ~95 to ~1%), followed by a humidification process (by increasing RH from ~1 to ~95%). The particles in the levitation system experienced a humidification process first (by increasing the RH from ~10 to ~80%) after quenching from droplets, followed by a dehydration process (by decreasing RH from ~80 to ~10%). The deposited particles (~6.5 μm size in average in this study) may have some influences from the collecting substrate such as a facilitated heterogeneous nucleation, which can be eliminated in the levitation system due to the substrate-free and contactless properties. However, the particles in the levitation system are generally large in size (~80 μm

in average in this study), which is less atmospherically relevant. And thus, the analysis of the particles in both systems is expected to give more detailed information on the hygroscopic behavior of MBTCA aerosols. NaCl, one of the major components of marine aerosols, was selected as the inorganic component since it was previously reported that organic acids contributed significantly to Cl depletion through a reaction with NaCl (Laskin et al., 2012). In situ Raman analysis could clearly identify MBTCA and its sodium salts during the hygroscopicity measurement despite NaCl being Raman inactive. To the best of the authors' knowledge, this is the first study on the hygroscopic behavior and chemical reactivity of MBTCA and its sodium salts thus far. The results are expected to promote more precise thermodynamic models (Clegg et al., 2003). The phase transitions were observed by monitoring the size changes together with the Raman spectra evolutions of the aerosol particles as a function of the RH. RMS can provide information on chemical functional groups, water contents, molecular interactions, and phase states of the aerosol particles. Such data can help understand the hygroscopic behavior of complex aerosol particles better (Lee et al., 2008; Li et al., 2017; Wang et al., 2017). The molecular characterization of organic aerosols can provide better insights into the potential mechanisms of SOA formation and transformation (or aging) (Hallquist et al., 2009). Scanning electron microscopy (SEM)/energy-dispersive X-ray spectroscopy (EDX) mapping was used to examine the elemental composition distribution in effloresced particles.

2. Experimental Section

2.1 Sample preparation

Pure 0.3 M solutions of NaCl (>99.9% purity, Sigma-Aldrich) and MBTCA (98%, Toronto Research Chemicals, TCR) were prepared. The mixture solutions of MBTCA and NaCl were prepared with molar mixing ratios of MBTCA:NaCl = 1:1, 1:2, 1:3, and 2:1. Mono-/di-/tri-sodium MBTCA salt solutions were obtained by mixing MBTCA and NaOH (>99.9% purity, Sigma-Aldrich) with molar ratios of MBTCA:NaOH = 1:1, 1:2, and 1:3, respectively. A mixture solution of MBTCA and monosodium MBTCA salt with a molar mixing ratio of 1:1 was prepared as well. All the solutions were made by dissolving the chemicals in the ultrapure de-ionized (DI) water (18 MΩ, Millipore Direct-QTM). Aerosol particles were generated by nebulizing the solutions using a single jet atomizer (HCT4810) on the Si

wafer substrates (MTI Corporation, 99.999% purity). The size of the droplets examined at RH > 90% ranged from 1 to 15 μm.

2.2 In situ Raman microspectrometry (RMS) for particles deposited on a Si wafer

During the hygroscopic measurements, in situ RMS was performed under a controlled RH to observe the hygroscopic behavior, structural changes, and chemical compositional variations of the aerosols generated from the solutions. The apparatus consisted of three parts: (A) see-through impactor, (B) Raman microscope/spectrometer, and (C) humidity-controlling system. The Si wafer substrate was mounted on the impaction plate in the see-through impactor. A more detailed discussion of the impactor and humidity-controlling system can be found elsewhere (Gupta et al., 2015). Briefly, the RH inside the impactor was controlled by mixing dry and wet (saturated with water vapor) N_2 (99.999% purity) gases. The flow rates of total 4 $L \cdot min^{-1}$ of the dry and wet N_2 gases were controlled by two mass flow controllers to obtain the desired RH in the range of ~1−95%, which was monitored using a digital hygrometer (Testo 645). The digital hygrometer was calibrated using a dew-point hygrometer (M2 Plus-RH, GE) to provide RH readings with ±0.5% reproducibility. The Raman spectra and optical images of the aerosol particles were recorded by Labspec6 using a confocal Raman microspectrometer (XploRA, Horiba Jobin Yvon) equipped with a ×50, 0.5 numerical aperture objective (Olympus). An excitation laser with a wavelength of 532 nm and 6 mW power was used, and the scattered Raman signals were detected at specific RHs during the hygroscopic measurements using an air-cooled multichannel charge-coupled device (CCD) detector. The data acquisition time for each measurement was 120 s. The spectral resolution was 1.8 cm^{-1} using 1800 gr/mm. The optical images were recorded continuously in RH = 1% steps with a size of 904×690 pixels during the first dehydration (by decreasing RH from ~95 to ~1%), followed by the humidification (by increasing RH from ~1 to ~95%) experiments using a top video camera assembled in the Raman instrument and processed using an image analysis software (Matrox, Inspector v9.0). Each humidity condition was sustained for at least 2 mins in order to provide an enough time for condensing or evaporating of water. The changes in particle size with the RH were monitored by measuring the particle 2-D area in the optical images to generate hygroscopic curves. These curves are represented by the area ratio (A/A_0) as a function of RH, where the 2-D projected aerosol area at a given RH (A) is divided

by that at the end of the dehydration process (A_0) (Ahn et al., 2010). All hygroscopic experiments were conducted at room temperature (T = 22±1℃). Aerosol particles generated from a pure NaCl aqueous solution to check the accuracy of the system showed typical hysteresis curves with deliquescence RH (DRH) = 75.5(±0.5)% and efflorescence RH (ERH) = 46.3–47.6% as shown in Fig. S2, which are consistent with the theoretical and reported values.

2.3 SEM/EDX X-ray mapping of effloresced particles deposited on Si wafer

SEM/EDX X-ray mapping was performed for effloresced particles to determine the morphology and spatial distribution of the chemical elements after the hygroscopicity measurements of individual particles (Ahn et al., 2010; Gupta et al., 2015). The measurements were carried out using a Jeol JSM-6390 SEM equipped with an Oxford Link SATW ultrathin window EDX detector. The resolution of the detector was 133 eV for Mn Kα X-rays. The X-ray spectra and elemental X-ray maps were recorded under the control of Oxford INCA Energy software. A 10 kV accelerating voltage and 0.7 nA beam current were used, and the typical measuring time for the elemental mapping was five minutes. An elemental quantification procedure, which is well described elsewhere (Wu et al., 2019a), was used for obtaining the elemental concentration.

2.4 In situ RMS assembled with a levitation system

The levitation experimental set up consisted of coupling an acoustic (ultrasonic) levitator equipped with an environmental cell to an RMS, as shown in Fig. S1. The theory of acoustic levitation is described in detail elsewhere (Seaver et al., 1989). An ultrasonic levitator was modified (APOS BA 10, Tec5, Germany) to be installed within an environmental levitation cell consisting of two quartz windows, allowing the particle analysis (Seng et al., 2018). Two inlet/outlet valves were used for gas supplies to modify the relative humidity (RH) inside the cell. A sensor (SHT75 Sensirion) was placed in the cell to control the RH and temperature. The RH inside the chamber was controlled by mixing dry and wet Ar gases with a flow rate of 200 $mL \cdot min^{-1}$ in the range of 10-80%(±1%) RH, and the temperature was T = 25±3 °C, making the experiments close to static flow conditions. The control of humidity and temperature allows limited droplet evaporation and long-term monitoring of the particles. The RMS measurements

were performed with a LabRAM HR Evolution confocal spectrometer (Horiba Scientific, S.A) at certain RHs first during humidification and then during dehydration. The instrument was equipped with an ×50, 0.45 numerical aperture Olympus objective (WD = 13.8 mm) and a He-Ne laser (λ = 632.8 nm – 6 mW) with a theoretical lateral resolution of ~2 μm, and a depth of the laser focus corresponding to 16 μm with a Δz limit ≥ ±3 μm. The cell was mounted on an XYZ stage under the objective, allowing an adjustment of the droplet in the optimal position for the measurements. The mean size of the initial droplet injected in the levitator was 80 μm. The Raman spectra and optical images recorded at specific RHs were analyzed similarly to those obtained on the Si wafer.

2.5 Measurement of acid dissociation constants of MBTCA

MBTCA is a tri-carboxylic acid with three acid dissociation constants. To determine the three constants, a 0.02 M, 5 ml MBTCA solution was titrated with a 0.1 M NaOH solution, where the constants were determined based on the Henderson-Hasselbalch equations (Harris, 2012):

$H_3M + OH^- \rightarrow H_2M^- + H_2O \quad pH = pKa_1 + \log([H_2M^-]/[H_3M])$

$H_2M^- + OH^- \rightarrow HM^{2-} + H_2O \quad pH = pKa_2 + \log([HM^{2-}]/[H_2M^-])$

$HM^{2-} + OH^- \rightarrow M^{3-} + H_2O \quad pH = pKa_3 + \log([M^{3-}]/[HM^{2-}])$

where H_3M, H_2M^-, HM^{2-}, and M^{3-} represent aqueous MBTCA, mono-, di-, and tri-sodium MBTCA anions, respectively. The pKa_1, pKa_2, and pKa_3 are the pHs when $[H_3M]$, $[H_2M^-]$, and $[HM^{2-}]$ equal $[H_2M^-]$, $[HM^{2-}]$, and $[M^{3-}]$, respectively, during the acid-base titration. Specifically, when NaOH was added at 0.5, 1.5, and 2.5 ml, the corresponding pHs of the solution are the three constants, which were 3.59, 4.85, and 6.79. Fig. 1 shows the calculated titration curve of MBTCA using the three determined Ka values, which is the same as the experimentally obtained titration data, supporting the validity of the Ka values, which were not reported so far.

3. Results and Discussion

3.1 Hygroscopic behavior of pure MBTCA particles

Wet-deposited MBTCA aerosols generated by the nebulization from a pure MBTCA solution exhibited three different types of hygroscopic behaviors, which are termed as “types 1, 2, and 3”. As

shown in Fig. 2, during the dehydration process, the exemplar droplets of types 1 and 2 shrank continuously with decreasing RH due to water evaporation until RHs = 58.4% and 40%, and then effloresced promptly at RH = 57.8% and gradually at RH = 39 - 35%, respectively. The effloresced particles maintained their size and shape with further decreases in RH. Whereas, the type 3 aerosols decreased continuously in size without a distinct change from RH = 94% to RH = 3% during the dehydration process. During the humidification process, types 1 and 2 particles kept the same size and shape until RH = ~90%, while type 3 particles experienced a gradual shrinkage at RH = 34-36.7% and remained the same until RH = ~85%. Fig. 2 also presents the corresponding optical images and in situ Raman spectra to assess the structural evolution of the MBTCA aerosols during the dehydration and humidification processes. Briefly, Raman peaks at ~1411 - 1420 cm^{-1}, ~1460 and ~2950 cm^{-1}, ~1660 - 1730 cm^{-1}, and ~3420 - 3475 cm^{-1} are for vibrations of C=O from COO^-, CH, C=O from COOH, and OH from water, respectively (Edsall, 1937; An et al., 2016). The redshift of the C=O peak (from COOH) from 1715 to 1660 cm^{-1} with decreasing FWHH (full width at half height), which is consistent with the standard MBTCA crystal, and the irregular shape and rough surface of types 1 and 2 aerosols at RH = 57.8% and 35%, respectively, confirmed that the particles effloresced into a solid phase. The optical images in the inset above the hygroscopic curve of the type 2 particles showed gradual efflorescence at RH = 39 – 35%. The water peak at ~3475 cm^{-1} disappeared as well after the efflorescence. In contrast, type 3 aerosols maintained a circular morphology until RH = 3%, as shown in the optical images in Fig. 2, even though an overlapped C=O (from COOH) peak at 1660 - 1680 cm^{-1} appeared during the dehydration process, and the water peak became undetectable, as shown in the Raman spectra at RHs = 45% and 3%, suggesting an amorphous/solid-state and the presence of an activation barrier or diffusional resistance to homogeneous nucleation required for the crystallization of MBTCA droplets as efflorescence is a kinetically controlled process (Martin, 2000; Freedman, 2017). Previous studies reported that α-pinene SOAs were very likely to exist as a highly viscous semisolid or even glassy state at low humidity (Saukko et al., 2012; Renbaum-Wolff et al., 2013; Berkemeier et al., 2014; Dette et al., 2014; Kidd et al., 2014; Song et al., 2016; Lessmeier et al., 2018). In addition, many organic substances, such as carboxylic acids, carbohydrates, and proteins, tend to form amorphous rather than crystalline phases upon the drying of aqueous solution droplets (Mikhailov et al., 2009). During the humidification process, the Raman spectra

and morphology remained unchanged for types 1 and 2 particles until RH = ~90%, where a slight decrease in morphology was observed due to structural re-arrangements by the absorption of moisture on the lattice imperfections (Gysel et al., 2002). Besides, the substrate can also affect this shrinkage. Especially, the hydrophilic substrate (such as Si wafer used in this study) seems to favor the phenomenon (Eom et al., 2014). Type 3 particles during the humidification process became irregular in shape, and the overlapped C=O (from COOH) peak shifted to 1660 cm^{-1} at RH = 36.7%, as shown in the optical image and Raman spectrum, indicating the formation of solids. With the further increase in RH, particles maintained their size and shape until RH = 85%, where they started to decrease in size due to a re-arrangement in structure. All types of MBTCA particles maintained the crystal phase until RH = 95%.

Specifically, the types of hygroscopicity of pure MBTCA particles were classified as, "type 1: with a prompt efflorescence at ~50% RH during dehydration; type 2: with a gradual efflorescence at ~35% RH during dehydration; type 3: with a gradual efflorescence at ~37% RH during humidification", based on their different behavior when efflorescence occurred. The different efflorescence behavior was attributed to different nucleation mechanisms: heterogeneous nucleation for types 1 and 2 particles (seed-containing), and homogeneous nucleation for type 3 particles (pure). MBTCA powders, which was used for making the MBTCA solution, has intrinsic unknown impurity of 2%, and they were used without any purification. When MBTCA powders were dissolved in DI water and particles were generated by the nebulization of the aqueous solution using N_2 gas, impurities were either absent or associated with the droplets. The impurities existed in types 1 and 2 particles after nebulization, acting as seed crystals to induce efflorescence. Aqueous moieties in particles were reported to effloresce more easily by heterogeneous nucleation in the presence of seeds (Schlenker and Martin, 2005; Li et al., 2014; Gupta et al., 2015). The lower ERH and gradual efflorescence of type 2 compared to type 1 particles might be due to the less amount of impurities. Type 3 particles contain negligible or no seed crystals, and large kinetic barrier and/or diffusional resistance make the formation of the crystal structure difficult owing to the decreasing availability of condensed water during dehydration, so that they did not experience any efflorescence. A similar situation was observed for NH_4NO_3, $NaNO_3$, and NH_4HSO_4 particles (Lightstone et al., 2000; Hoffman et al., 2004; Gibson et al., 2006; Kim et al., 2012; Jing et al., 2018; Sun et al., 2018; Wu et al., 2019b). The Si substrates used in this study could also facilitate efflorescence (Eom et al., 2014;

Wang et al., 2017). The efflorescence during humidification like type 3 particles was previously reported for Amazonian rain forest aerosols (Pöhlker et al., 2014) and the laboratory-generated NaCl–$MgCl_2$ mixture particles (Gupta et al., 2015). Thus, this phenomenon is not rare. And it was claimed that the aerosol particles initially had amorphous or poly-crystalline structures and underwent restructuring through kinetic water and ion mobilization in the presence of sufficient condensed water, resulting in overcoming the kinetic barrier and crystallization during humidification.

Among 100 particles, type 1-3 particles accounted for approximately 25%, 5%, and 70%, respectively, suggesting that MBTCA has slow homogeneous nucleation rate. Based on the experimental results, MBTCA droplets have DRH > 95% and ERH = 30–58%. This is the first study reporting the hygroscopic properties of MBTCA. A previous study showed that MBTCA was not hydrated significantly in the ambient atmosphere (Kildgaard et al., 2018), and our results also implied that the MBTCA solids stay in the air once they effloresced, based on our results.

3.2 Hygroscopic behavior of mono-/di-/tri-sodium MBTCA salt aerosols

The hygroscopicity and Raman spectra of mono-/di-/tri-sodium MBTCA salt aerosols (hereafter, denoted as NaH_2M, Na_2HM, and Na_3M, respectively) were studied to examine the hygroscopic behavior and estimate the chemical reactivity of MBTCA with NaCl. Figs. 3(a)-(c) show the 2-D projected area ratio plot of aerosol particles generated from 0.3 M NaH_2M, Na_2HM, and Na_3M aqueous solutions as a function of the RH together with the corresponding optical images and Raman spectra recorded at specific RHs. As shown in Figs. 3(a) and (b), NaH_2M and Na_2HM aerosols shrank and grew continuously without a phase transition during the dehydration and humidification processes, respectively, which is also reflected in the optical images and Raman spectra, where they maintained their circular morphology only with a change in size and the same Raman peak patterns and positions with small variations in the relative peak intensities during the entire process. The water peak at ~3400-3500 cm^{-1} can still be observed at the end of the dehydration process. Even after being kept in a desiccator for two months, NaH_2M and Na_2HM particles still showed the same shapes and Raman spectra with those at RHs = 3.4% and 2.8%, respectively. These results indicate the non-crystallizable properties and supersaturated amorphous phase state of the particles. The Na_3M particles behaved differently as they did not crystallize during the

dehydration process. On the other hand, the aerosols exhibited efflorescence at RH = 46.8% during the humidification process (Fig. 3(c)), deliquesced to become a droplet at RH = 53.1%, and grew continuously after that with increasing RH. The Raman spectra of the Na_3M particles in Fig. 3(c) showed that the peak at 1420-1460 cm^{-1} became two sharp peaks when the particles effloresced, and the OH peak at 3400 cm^{-1} indicates that Na_3M particles possibly exist in the hydrated form. The Na_3M particles behaved analogously to type 3 MBTCA particles, which might be due to their similar structures when all three COOH in MBTCA were replaced with COONa upon the reaction between MBTCA with NaOH. Since all the observed Na_3M particles on the substrate (around 100 particles) behaved exactly in the same way with crystallization during humidification process, the major contribution to the crystallization of Na_3M particles is homogeneous crystallization, instead of heterogeneous crystallization induced by impurities and Si substrate effect. Based on the top Raman spectra of aqueous MBTCA, NaH_2M, Na_2HM, and Na_3M aerosols in Figs. 2 and 3, the ratios of the CH peak at ~1460 cm^{-1} to the C=O peak at ~1720 cm^{-1} (from COOH) and to the C=O peak at ~1420 cm^{-1} (from COO^-) increased and decreased in the order of MBTCA, NaH_2M, Na_2HM, and Na_3M because of their reduced and elevated levels of COOH and COO^-, respectively.

3.3 Hygroscopic behavior of MBTCA-NaCl mixture aerosols

Aerosols were generated by the nebulization of MBTCA-NaCl mixture solutions of molar mixing ratios of MBTCA:NaCl = 1:1, 1:2, 1:3, and 2:1 and deposited on Si wafer substrates, while maintaining the entire hygroscopic measurement system at RH > 90%. The hygroscopic behavior was investigated for ~10 individual aerosols of each mixing ratio, which are discussed in the following sections.

3.3.1 Aerosols generated from solutions of MBTCA:NaCl = 1:1 and 2:1

Fig. 4 presents the hygroscopic curves of representative aerosols nebulized from solutions of MBTCA:NaCl mixtures at different molar ratios (1:1 and 2:1) along with the corresponding optical images and Raman spectra at specific RHs. During the dehydration process, the circular liquid droplets decreased in size gradually without any noticeable phase change. The Raman peak patterns were maintained only with the C=O peak at 1721 cm^{-1} (from COOH) shifting mildly rightwards, the water peak

at 3466 cm^{-1} becoming undetectable, and the relative peak intensities at ~1411, 1457, and 1721 cm^{-1} varied when the RH was as low as 1.2%, indicating that the liquid droplets formed amorphous solids. The peak at 1680 cm^{-1} on the Raman spectra of MBTCA:NaCl = 2:1 at RH = 1.2% suggested that the amorphous structure of the remaining MBTCA had been retained. Both MBTCA and NaCl have their DRHs and ERHs. Therefore, a step-wise efflorescence would happen if it is assumed that the mixture aerosols are an MBTCA-NaCl binary system, i.e., a component of the aqueous droplets precipitates first at their specific ERHs depending on their mixing ratios, and the second crystallization from the remnant eutonic solution occurs at their mutual ERH (MERH) with further decreases in RH, which is independent of the mixing ratios, generally forming a heterogeneous, core-shell crystal structure owing to the two-stage crystallization process (Ge et al., 1996; Gupta et al., 2015). However, the particles of MBTCA:NaCl = 1:1 and 2:1 mixing ratios did not follow the step-wise transitions in the present study, revealing that the aerosols do not belong to the MBTCA-NaCl binary system and the chemical compositions evolved during the hygroscopic experiment due to the reaction between MBTCA and NaCl, which will be discussed later.

During the humidification process, aerosol particles of two mixing ratios grew continuously when the RH was increased from 1.2% to 90% with C=O peak (from COOH) shifting back to ~1721 cm^{-1} and the water peak becoming significant, as shown in Fig. 4. Several small crystal-like spots, which are marked by a dotted circle on the inset optical image beside the hygroscopic curve in Fig. 4(a), appeared in the particles with the mixing ratio of MBTCA:NaCl = 1:1 when the RH was increased to 67.2% and dissolved completely at RH = 71.2%. As the Raman spectra did not show any signals of the crystallized organics and RH = 71.2% is close to the DRH of pure NaCl (75(±0.5)%), the crystal-like moieties should result from the effloresced NaCl. The more noticeable water peak in the Raman spectrum taken at RH = 71.2% than that at RH = 67.2% also supports that the NaCl dissolved at RH = 71.2% as NaCl is quite hygroscopic (Li et al., 2017). No phase transition of NaCl was detected during the dehydration process, probably because the supersaturated organic moiety inhibited the crystallization of NaCl. The observation of effloresced particles during the humidification process might be caused by the structural re-arrangement of the amorphous particles upon the slow and continuous absorption of moisture with increasing RH (Mikhailov et al., 2009), leading to less restriction to NaCl crystallization. Indeed, organics in organic-inorganic mixture aerosols were reported to be a minor disturbance to the DRH of inorganic salts; in

contrast, they may markedly decrease the ERH of inorganic salts depending on the organic type (Parsons et al., 2004).

3.3.2 Aerosols generated from solutions of MBTCA:NaCl = 1:2 and 1:3

Fig. 5 shows the hygroscopic curves of aerosol particles nebulized from solutions of MBTCA:NaCl with molar mixing ratios of 1:2 and 1:3, together with the corresponding optical images and Raman spectra at the transition RHs. During the dehydration process, droplets from the solutions of MBTCA:NaCl = 1:2 and 1:3 decreased gradually in size owing to water evaporation until a single-stage transition was observed at RHs = 47.2-46.5% and 46.7-45.8%, respectively, where the particle shape became less circular in the optical images. At this point, the following were observed in the Raman spectra: the water peak at 3455 cm^{-1} disappeared; the C=O peak at ~1722/1720 cm^{-1} (from COOH) shifted slightly rightwards; the relative peak intensities at 1417/1416, 1461, and 1722/1720 cm^{-1} varied. With the further decreases in RH until ~6%, the particles kept their size and shape. During the humidification process, all particles of MBTCA:NaCl = 1:2 and 1:3 maintained their structure until RHs = 50% and 40%, respectively, where they experienced a size decrease due to structural re-arrangement until RH = ~70%, grew continuously to become circular at RH = ~73%, and totally deliquesced into homogeneous droplets at RHs = 73.9% and 74.5%, respectively. Particle size and water peak increased rapidly, and the C=O peak (COOH) shifted back to 1720 cm^{-1}. Upon a further increase in RH, they grew continuously by water absorption. The ERH and DRH were attributed to the NaCl moiety as the Raman spectra maintained the peak patterns during the entire process, and the organic components condensed onto the NaCl crystal core almost simultaneously as an amorphous shell when efflorescence occurred, which is also indicated by the optical images. Before the complete deliquescence of the NaCl crystal core, the water peak at ~3455 cm^{-1} in the Raman spectra and the optical images at RH = 72.4% and 73.8% of the particles from the MBTCA:NaCl = 1:2 and 1:3 solutions show that the organic shell was in the liquid phase, meaning that the mixture particles were in a solid-liquid equilibrium state (Sun et al., 2018). The Raman spectra shown in the figures were all obtained in the center of the particles. The Raman spectra were obtained both at the center and the edge of the particles for comparison during the measurement when the heterogeneity appeared during the hygroscopic measurements. The spectra from the center and the edge were different

only in the intensity since NaCl is Raman inactive. As shown in the Fig. S3, the Raman spectra which were obtained from the center and the edge of an exemplar MBTCA:NaCl = 1:3 particle during the humidification process, match well after normalization to the CH peak at 1460 cm^{-1}.

All the particles from MBTCA:NaCl = 1:2 and 1:3 solutions showed hysteresis curves with ERHs in the range of 46.7-45.2% and 47.2-45.6%, respectively, and DRHs = 73.9(±0.3)% and 74.5(±0.3)%, respectively.

3.3.3 Chemical reactivity of aerosols generated from MBTCA−NaCl mixture solutions

The first Raman spectra of the aerosols generated from MBTCA-NaCl mixture solutions in Figs. 4 and 5 were obtained before the dehydration process, which are comparable to that of pure MBTCA droplet particle in Fig. 2 except for a much stronger free water peak at 3450-3470 cm^{-1} due to the presence of a more hygroscopic NaCl moiety. This suggests that upon nebulization from the solutions, the mixture droplets were mostly the MBTCA-NaCl binary system. The Raman spectra obtained at the beginning of the dehydration process and the end of the humidification process revealed increased and decreased ratios of the CH peak at ~1460 cm^{-1} to the C=O peaks at ~1720 cm^{-1} (from COOH) and ~1412 cm^{-1} (from COO^-), respectively, which implies that the reaction between MBTCA and NaCl occurred during the hygroscopic experiment, leading to the decreased and increased levels of the COOH and COO^- moieties, respectively. It is worth noticing that the dehydration and humidification curves of the MBTCA-NaCl mixtures did not overlap with each other mainly because of the different amounts of NaCl in the dehydration and humidification processes. As shown in the Fig. S2, NaCl is quite hygroscopic with around four times change in 2-D area after deliquescence, so the decreased amount of NaCl in the mixtures also lead to the smaller 2-D area when the MBTCA-NaCl mixture particles experienced hygroscopic growth during the humidification process, compared to those before dehydration. Fig. 6(a) presents the Raman spectra of particles generated from MBTCA:NaCl = 1:1, 1:2, and 1:3 solutions together with that of NaH_2M particles obtained at the end of humidification by normalizing to the CH peak at 1458 cm^{-1}. The C=O peak intensities at 1720 cm^{-1} (from COOH) and 1412 cm^{-1} (from COO^-) of the particles generated from the mixture solutions were higher and lower, respectively, than those of the NaH_2M particle, suggesting that the aerosols generated from the MBTCA-NaCl solutions produced only NaH_2M

as the reaction product between MBTCA and NaCl, regardless of the mixing ratios. The droplet particles after the humidification process were present as an MBTCA-NaCl-NaH_2M ternary system with varying compositions. As the first acid dissociation constant of MBTCA ($pKa_1 = 3.59$) is more than 1 and 3 orders of magnitude larger than the second ($pKa_2 = 4.85$) and third ($pKa_3 = 6.79$), respectively, H_2M^- is more abundant than HM^{2-} and M^{3-}. The chemical reaction between NaCl and MBTCA would occur in the aqueous phase as follows:

$$MBTCA(aq) + H_2M^-(aq) + H^+(aq) + Na^+(aq) + Cl^-(aq) \rightarrow MBTCA(aq) + H_2M^-(aq) + Na^+(aq) + Cl^-(aq) + HCl(g)\uparrow \rightarrow NaH_2M\ (+ MBTCA, amorphous) + NaCl(s)\ after\ the\ efflorescence$$

The NaH_2M particles may exist as amorphous particles, as described before in section 3.2. Raman spectra of standard aerosols generated from solutions of MBTCA:NaH_2M = 0:1, 1:1, and 1:0 were obtained at different RHs to estimate the chemical reactivity of the aerosol particles generated from the MBTCA-NaCl mixture solutions, which were used as a calibration curve to help determine the relative MBTCA and NaH_2M contents in the aerosols at specific RHs. The estimation of the chemical reactivity between malonic acid and NaCl performed in the similar way was reported in a previous study (Li et al., 2017). The Raman spectra of MBTCA, NaH_2M, and mixture aerosols of MBTCA:NaH_2M = 1:1 obtained at RH = 90% and normalized to the CH_3 peak at 1460 cm^{-1} showed that the intensity ratio of the two peaks at 1460 cm^{-1} (CH_3) and ~1720 cm^{-1} (C=O from COOH) (i.e., I_{1460}/I_{1720}) increased with increasing NaH_2M level because of the decreased COOH content, as shown in Fig. 6(b). The ratio, I_{1460}/I_{1720}, for each standard aerosol exhibited good linearity as a function of RH, as shown in Fig. 7(a), where the mean values obtained from 10 aerosols of each standard aerosol sample are plotted with error-bars. The Raman intensity ratios of the standard aerosols increased with decreasing RH because the C=O stretching vibrations of the free COOH group in the aqueous phase and the intramolecular hydrogen-bonded COOH group in the supersaturated phase become weaker and stronger (Bertran et al., 2010), respectively, with decreasing RH during the dehydration process.

The dependency of the I_{1460}/I_{1720} ratios on RH can be used to estimate the MBTCA and NaH_2M (monosodium MBTCA salt) contents in the NaCl-MBTCA aerosols at specific RHs based on the

calibration curve and to calculate the further reactivity. The chemical reactivity of the mixtures is represented as the degree of the reaction, which is defined as the ratio of consumed to the original amount of the limiting reactant. For example, for aerosols from solutions of MBTCA:NaCl = 2:1 and 1:2, NaCl and MBTCA are the limiting reactants, respectively. Fig. 7(b) shows the degree of the reaction of aerosols generated from solutions of each mixing ratio, where the mean degree of reaction has ~1.5-4% deviations owing to statistical variations in the Raman peak intensities caused by the baseline correction procedure and the uncertainties involved in the calibration measurements. The reactivity was estimated at five stages during one cycle hygroscopic experiment.

Stage 1; At the beginning of the hygroscopic experiment, no reaction occurred for all the mixed droplets based on their Raman spectra, i.e., the degree of the reaction is 0.

Stage 2; As the RH decreased during the dehydration process, the reaction continued in the aqueous aerosols until efflorescence of the droplets with mixing ratios of MBTCA:NaCl = 1:2 and 1:3 had occurred, and until the water content of the aerosols with mixing ratios of MBTCA:NaCl = 1:1 and 2:1 became insignificant. The degrees of the reaction of aerosols with mixing ratios of 1:1, 1:2, and 1:3 were approximately 30%, whereas that of 2:1 approached 85%.

Stage 3; The reaction of aerosols generated from the solution of mixing ratio of MBTCA:NaCl = 2:1 was complete at the end of the dehydration process, indicating the total consumption of NaCl and the formation of an MBTCA:NaH_2M = 1:1 mixture aerosol. The Raman spectra of the aerosols with mixing ratios of MBTCA:NaCl = 1:1, 1:2, and 1:3 at the end of the dehydration process were unsuitable for the reactivity estimation mostly due to their heterogeneous structure in the presence of a NaCl core.

Stages 4 and 5; The reaction proceeded after deliquescence when the free H^+ and Cl^- became available again for aerosols with mixing ratios of MBTCA:NaCl = 1:1, 1:2, and 1:3, and a small

increase in the degree of reaction (~5%) was observed at the end of humidification for these mixture droplets.

Most of the reactions occurred in the aqueous phase during the dehydration process with considerable amounts of aqueous H^+ from MBTCA and Cl^- from NaCl available for HCl liberation. During the entire experiment, the reactivity followed the sequence of MBTCA:NaCl = 2:1 > 1:3 > 1:2 > 1:1, where the reactivity appeared to be enhanced when either of the reactants is enriched. On the other hand, the reaction was complete only when aqueous H^+ was sufficiently available, i.e., the reaction depended mostly on the triacid level. The real-time aerosol mixture components based on the reactivity estimation of each mixing ratio at specific RHs are shown on the hygroscopic curves in Figs. 4 and 5.

The morphology and elemental distribution of effloresced MBTCA-NaCl particles were examined by SEM/EDX. Figure 8(a) shows the secondary electron images (SEIs) of the exemplar particles of each mixing ratio. The elemental X-ray maps for MBTCA:NaCl = 1:1 and 1:2 particles suggest that the NaCl solid moiety (represented by Na and Cl X-ray maps) crystallized homogeneously at small spots inside the organic moiety. For MBTCA:NaCl = 1:3 particles with a significant amount of NaCl, the NaCl solid existed as a core surrounded by the organic moiety. The organic mixture of MBTCA and NaH_2M (represented by C and Na) condensed onto the NaCl core almost simultaneously when efflorescence occurred, while maintaining a relatively circular morphology, even after being inserted into the vacuum SEM chamber, which also indicates the low crystallization tendency of the organic moiety. The different shapes of organic shell-inorganic core structures depending on the organic mass fraction and RH are reported elsewhere (Karadima et al., 2019). The homogeneous structure of C and Na and the absence of Cl for particles with mixing ratios of MBTCA:NaCl = 2:1, as shown in the corresponding SEIs and X-ray spectrum in Figs. 8(a) and (b), confirmed that the reaction was complete at the end of the dehydration process. The reaction between MBTCA and NaCl and the changes in the microstructures after the reaction are expected to have some atmospheric implications since they may have enhanced ability to facilitate further heterogeneous reactions in the atmosphere because of their low crystallization property. Na (from both NaH_2M and NaCl) and Cl (from NaCl) levels were used to estimate the degrees of reaction for the

MBTCA:NaCl = 1:1, 1:2, 1:3, and 2:1 systems, which were estimated to be ~25%, ~30%, ~37%, and 100%, respectively, with well matching to those from the Raman analysis by 5-8% differences.

3.4 Hygroscopic behavior of pure MBTCA and MBTCA−NaCl mixture particles in the levitation system

The data acquired from the levitation system for contactless experiments on particles of ~80 μm were used to compare with those obtained for aerosols on the Si wafer in the see-through impactor. The droplets were introduced into the levitator and dried rapidly at RH = ~10% within 15 minutes (first rapid dehydration, i.e., a quenching process), and humidified progressively to RH = 80%. Once RH = 80%, the particles were dehydrated gradually until RH = ~10% (second dehydration).

Two types of hygroscopic behavior of pure MBTCA particles were observed, corresponding closely to types 1 and 3 aerosol particles in the see-through impactor system, due to heterogeneous crystallization induced by impurity seed crystals and homogeneous crystallization, respectively, confirming that once the MBTCA particles overcome the kinetic barrier and effloresce into solids, they no longer capture water significantly. The ERH was ~49-54%. The Raman spectra and optical images are not shown separately.

The Raman spectra and optical images of particles composed of MBTCA:NaCl = 1:1, 1:2, and 1:3 mixing ratios are shown in Fig. 9. After the first rapid dehydration of the particles, the existence of peaks at 1655 and 1720 cm^{-1} was observed for all the mixtures, and the relative intensity of the peak at ~1720 cm^{-1} increased with the increase of the NaCl content, suggesting the formation of the mixture of solid MBTCA and amorphous moiety either from MBTCA or NaH_2M. During the humidification process, the Raman peak at 1720 cm^{-1} and the particle size grew continuously with increasing RH. Transitions were observed at RH = ~71%, ~74.5%, and ~75% for MBTCA:NaCl = 1:1, 1:2, and 1:3 mixture particles, respectively, with the water peak at ~3500 cm^{-1} becoming significant for the three compositions. The observed transition points were attributed to the deliquescence of NaCl within the particle with the MBTCA moiety partially remaining as a solid phase, and the elevated NaCl content strongly enhanced the ability of the particles to uptake water. The peak related to the solid portion at 1655 cm^{-1} disappeared only for the MBTCA:NaCl = 1:3 mixture particles at the end of humidification, suggesting that the particle had transformed completely into a droplet. During the second dehydration process, the particles showed

528 the entire release of water, as illustrated by the disappearance of the peak at 3500 cm^{-1} at RH = ~50%,
529 i.e., the ERH, for all the mixtures while maintaining the peak patterns and positions until the lowest RH.
530 The Raman spectra recorded at the end of dehydration revealed both solid and amorphous phases for the
531 MBTCA:NaCl = 1:1 and 1:2 mixtures due to the existence of the peaks at 1655 and 1720 cm^{-1}. In contrast,
532 only the 1720 cm^{-1} associated with the amorphous composition was observed for the MBTCA:NaCl =
533 1:3 mixture, suggesting that the reaction between MBTCA and NaCl was facilitated extensively by the
534 increased NaCl concentration while absorbing sufficient moisture. The conspicuous DRHs and ERHs of
535 all the mixtures in the levitation system demonstrated a smaller degree of reaction between MBTCA and
536 NaCl compared to those obtained in the see-through impactor, which might be caused by the relatively
537 closed atmosphere in the levitator as the default settings of N_2 flow inside the see-through impactor cell
538 and the levitation cell were 4 and 0.2 $L \cdot min^{-1}$, respectively, i.e., less release of HCl. The larger size of the
539 levitated particles could limit the release of HCl (Kerminen et al., 1997). In addition, the quenching
540 process, i.e., the starting point of the hygroscopicity experiments, induced the solidification of MBTCA,
541 and further, a slow reaction between MBTCA and NaCl.
542
543 **4. Conclusions and atmospheric implication**
544 The hygroscopic behavior, physical states, and chemical reactivity of pure MBTCA particles, mono-
545 /di-/tri-sodium MBTCA salt particles, and MBTCA-NaCl particles of different mixing ratios were
546 examined by in situ RMS assembled with a see-through impactor as the starting point with dehydration.
547 The DRHs and ERHs of the laboratory-generated particles in the micrometer size range at room
548 temperature were determined by monitoring the change in the particle area in the 2-D optical images and
549 the corresponding Raman spectra at transition points with RH variation of ~1-95%. Pure MBTCA showed
550 three types of hygroscopic behaviors in that types 1 and 2 particles effloresced suddenly and gradually,
551 respectively, at ERH = 30-58% during the dehydration process, whereas type 3 particles crystallized
552 during the humidification process at RH = ~37%, not during the dehydration process because of a kinetic
553 barrier to nucleation with limited condensed water. Subsequently, all particles maintained their crystal
554 structure until RH = 95%. The mono- and di-sodium MBTCA salt aerosols did not show a clear ERH and
555 DRH during the dehydration and humidification processes, respectively. In contrast, the tri-sodium

MBTCA showed ERH = ~44.4-46.8% (during humidification) and DRH = ~53.1%. The MBTCA-NaCl droplets with molar mixing ratios of MBTCA:NaCl = 1:1 and 2:1 showed no distinct DRH and ERH because of the partial and complete reactions with NaCl, respectively, whereas those with ratios of MBTCA:NaCl =1:2 and 1:3 experienced single-stage efflorescence and deliquescence governed by the excess NaCl. Only monosodium MBTCA (NaH_2M) could be formed as a result of the reaction between NaCl and MBTCA regardless of the mixing ratios, mostly during the dehydration process within the timescale of one to two hours according to Raman analysis, indicating that the MBTCA-NaCl mixture systems are in an MBTCA-NaH_2M-NaCl ternary system except when NaCl has reacted completely in the mixture aerosols of MBTCA:NaCl = 2:1 ratio. The MBTCA-NaH_2M existed as amorphous solids, even when the excess crystalline NaCl acted as a heterogeneous nucleation core, which was also confirmed by X-ray mapping. The reaction occurred more rapidly with a more elevated concentration of either MBTCA or NaCl, and the controlling factor for the reactivity of the mixtures depended mostly on the availability of H^+ dissociated from the MBTCA tricarboxylic acid. The hygroscopic experiments for pure MBTCA and MBTCA-NaCl mixture particles were also performed in a levitation system with the starting point from humidification after the quenching process and the RH variation of ~10 to 80%. The results acquired from the levitation system are consistent with those obtained from the see-through impactor, only with less reaction between MBTCA and NaCl resulting from the airtight atmosphere inside the levitator and the partial solidification of MBTCA after the quenching process. In addition, the elevated NaCl moiety can eventually transform the solidified MBTCA into droplets through reactions when absorbing adequate moisture.

These observations are expected to have important atmospheric implications in that they may help to better understand the complexity of real ambient SOA and inorganic mixture particles. In this study, the hygroscopicity of MBTCA was altered significantly when mixed with NaCl due to the reaction, so that they are more likely to contribute to further gas-particle interactions. The amorphous phase state may influence the uptake of gaseous photo-oxidants as well as the chemical transformation and aging of atmospheric aerosols (Mikhailov et al., 2009). The observed aqueous shell with the solid core upon the humidification of the mixture particles with mixing ratios of MBTCA:NaCl = 1:2 and 1:3 before the total dissolution of NaCl can scatter solar radiation more efficiently (Adachi et al., 2011; Sun et al., 2018). The

aerosol liquid water can promote heterogeneous aqueous-phase chemical processes, resulting in the facile formation of secondary aerosols (Cheng et al., 2016; Li et al., 2019). Recently, heterogeneous reactions in aerosol water were reported to be a significant mechanism for haze formation in North China (Sun et al., 2018). Overall, the hygroscopic curve, Raman signatures, and X-ray maps of the effloresced particles provided clear features of the hygroscopic behavior and chemical reactivity of the MBTCA-NaCl mixture system covered in this study. These results are expected to provide insights into the physicochemical characteristics and atmospheric chemistry of highly oxidized SOAs mixed with inorganic particles.

Data availability. The data used in this study are available upon request; please contact Chul-Un Ro (curo@inha.ac.kr).

Author contributions. LW, CB, SS, and CR designed the experiment. LW, CB, and SS carried out the measurements and/or analyzed the data. LW, CB, SS, PF, EP, EV, YS and CR contributed discussion of the data. LW, SS, and CR drafted the paper.

Competing interests. The authors declare that they have no conflict of interest.

Acknowledgments. This study was supported by Basic Science Research Programs through the National Research Foundation of Korea (NRF) funded by the Ministry of Education, Science, and Technology (NRF-2018R1A2A1A05023254) and by the National Strategic Project-Fine particle of the National Research Foundation of Korea (NRF) funded by the Ministry of Science and ICT (MSIT), the Ministry of Environment (ME), and the Ministry of Health and Welfare (MOHW) (2017M3D8A1090654). Authors thank the Region Nouvelle Aquitaine for the financial support of the SPECAERO project. This work was performed through international and collaborative programs supported by PHC STAR n° 38815XE and visiting scholars program from IDEX of the University of Bordeaux.

References

611 Adachi, K., Freney, E. J., and Buseck, P. R.: Shapes of internally mixed hygroscopic aerosol particles
612 after deliquescence, and their effect on light scattering, Geophysical Research Letters, 38, n/a-n/a,
613 10.1029/2011gl047540, 2011.
614 Ahn, K.-H., Kim, S.-M., Jung, H.-J., Lee, M.-J., Eom, H.-J., Maskey, S., and Ro, C.-U.: Combined use
615 of optical and electron microscopic techniques for the measurement of hygroscopic property,
616 chemical composition, and morphology of individual aerosol particles, Analytical chemistry, 82,
617 7999-8009, 2010.
618 Aljawhary, D., Zhao, R., Lee, A. K., Wang, C., and Abbatt, J. P.: Kinetics, Mechanism, and Secondary
619 Organic Aerosol Yield of Aqueous Phase Photo-oxidation of alpha-Pinene Oxidation Products, J
620 Phys Chem A, 120, 1395-1407, 10.1021/acs.jpca.5b06237, 2016.
621 An, P., Yuan, C.-Q., Liu, X.-H., Xiao, D.-B., and Luo, Z.-X.: Vibrational spectroscopic identification of
622 isoprene, pinenes and their mixture, Chinese Chemical Letters, 27, 527-534,
623 10.1016/j.cclet.2016.01.036, 2016.
624 Bateman, A. P., Bertram, A. K., and Martin, S. T.: Hygroscopic influence on the semisolid-to-liquid
625 transition of secondary organic materials, J Phys Chem A, 119, 4386-4395, 10.1021/jp508521c,
626 2015a.
627 Bateman, A. P., Gong, Z., Liu, P., Sato, B., Cirino, G., Zhang, Y., Artaxo, P., Bertram, A. K., Manzi, A.
628 O., Rizzo, L. V., Souza, R. A. F., Zaveri, R. A., and Martin, S. T.: Sub-micrometre particulate
629 matter is primarily in liquid form over Amazon rainforest, Nature Geoscience, 9, 34-37,
630 10.1038/ngeo2599, 2015b.
631 Berkemeier, T., Shiraiwa, M., Pöschl, U., and Koop, T.: Competition between water uptake and ice
632 nucleation by glassy organic aerosol particles, Atmospheric Chemistry and Physics, 14, 12513-
633 12531, 10.5194/acp-14-12513-2014, 2014.
634 Bernard, F., Ciuraru, R., Boreave, A., and George, C.: Photosensitized Formation of Secondary Organic
635 Aerosols above the Air/Water Interface, Environ Sci Technol, 50, 8678-8686,
636 10.1021/acs.est.6b03520, 2016.
637 Bertran, O., Armelin, E., Estrany, F., Gomes, A., Torras, J., and Alemán, C.: Poly (2-thiophen-3-yl-
638 malonic acid), a polythiophene with two carboxylic acids per repeating unit, The Journal of
639 Physical Chemistry B, 114, 6281-6290, 2010.
640 Cheng, Y., Zheng, G., Wei, C., Mu, Q., Zheng, B., Wang, Z., Gao, M., Zhang, Q., He, K., and Carmichael,
641 G.: Reactive nitrogen chemistry in aerosol water as a source of sulfate during haze events in China,
642 Science Advances, 2, e1601530, 2016.
643 Chu, B., Wang, K., Takekawa, H., Li, J., Zhou, W., Jiang, J., Ma, Q., He, H., and Hao, J.: Hygroscopicity
644 of particles generated from photooxidation of α-pinene under different oxidation conditions in the
645 presence of sulfate seed aerosols, Journal of Environmental Sciences, 26, 129-139,
646 10.1016/s1001-0742(13)60402-7, 2014.
647 Clegg, S. L., Seinfeld, J. H., and Edney, E. O.: Thermodynamic modelling of aqueous aerosols containing
648 electrolytes and dissolved organic compounds. II. An extended Zdanovskii–Stokes–Robinson
649 approach, Journal of aerosol science, 34, 667-690, 2003.
650 Cui, T., Green, H. S., Selleck, P. W., Zhang, Z., O'Brien, R. E., Gold, A., Keywood, M., Kroll, J. H., and
651 Surratt, J. D.: Chemical Characterization of Isoprene- and Monoterpene-Derived Secondary

Organic Aerosol Tracers in Remote Marine Aerosols over a Quarter Century, ACS Earth and Space Chemistry, 3, 935-946, 10.1021/acsearthspacechem.9b00061, 2019.
Dette, H. P., Qi, M., Schroder, D. C., Godt, A., and Koop, T.: Glass-forming properties of 3-methylbutane-1,2,3-tricarboxylic acid and its mixtures with water and pinonic acid, J Phys Chem A, 118, 7024-7033, 10.1021/jp505910w, 2014.
Ding, X., Wang, X.-M., Gao, B., Fu, X.-X., He, Q.-F., Zhao, X.-Y., Yu, J.-Z., and Zheng, M.: Tracer-based estimation of secondary organic carbon in the Pearl River Delta, south China, Journal of Geophysical Research: Atmospheres, 117, n/a-n/a, 10.1029/2011jd016596, 2012.
Donahue, N. M., Henry, K. M., Mentel, T. F., Kiendler-Scharr, A., Spindler, C., Bohn, B., Brauers, T., Dorn, H. P., Fuchs, H., Tillmann, R., Wahner, A., Saathoff, H., Naumann, K. H., Mohler, O., Leisner, T., Muller, L., Reinnig, M. C., Hoffmann, T., Salo, K., Hallquist, M., Frosch, M., Bilde, M., Tritscher, T., Barmet, P., Praplan, A. P., DeCarlo, P. F., Dommen, J., Prevot, A. S., and Baltensperger, U.: Aging of biogenic secondary organic aerosol via gas-phase OH radical reactions, Proc Natl Acad Sci U S A, 109, 13503-13508, 10.1073/pnas.1115186109, 2012.
Dunne, E. M., Gordon, H., Kurten, A., Almeida, J., Duplissy, J., Williamson, C., Ortega, I. K., Pringle, K. J., Adamov, A., Baltensperger, U., Barmet, P., Benduhn, F., Bianchi, F., Breitenlechner, M., Clarke, A., Curtius, J., Dommen, J., Donahue, N. M., Ehrhart, S., Flagan, R. C., Franchin, A., Guida, R., Hakala, J., Hansel, A., Heinritzi, M., Jokinen, T., Kangasluoma, J., Kirkby, J., Kulmala, M., Kupc, A., Lawler, M. J., Lehtipalo, K., Makhmutov, V., Mann, G., Mathot, S., Merikanto, J., Miettinen, P., Nenes, A., Onnela, A., Rap, A., Reddington, C. L., Riccobono, F., Richards, N. A., Rissanen, M. P., Rondo, L., Sarnela, N., Schobesberger, S., Sengupta, K., Simon, M., Sipila, M., Smith, J. N., Stozkhov, Y., Tome, A., Trostl, J., Wagner, P. E., Wimmer, D., Winkler, P. M., Worsnop, D. R., and Carslaw, K. S.: Global atmospheric particle formation from CERN CLOUD measurements, Science, 354, 1119-1124, 10.1126/science.aaf2649, 2016.
Edsall, J. T.: Raman Spectra of Amino Acids and Related Compounds IV. Ionization of Di- and Tricarboxylic Acids, The Journal of Chemical Physics, 5, 508-517, 10.1063/1.1750067, 1937.
Enami, S., and Sakamoto, Y.: OH-Radical Oxidation of Surface-Active cis-Pinonic Acid at the Air-Water Interface, J Phys Chem A, 120, 3578-3587, 10.1021/acs.jpca.6b01261, 2016.
Eom, H. J., Gupta, D., Li, X., Jung, H. J., Kim, H., and Ro, C. U.: Influence of collecting substrates on the characterization of hygroscopic properties of inorganic aerosol particles, Anal Chem, 86, 2648-2656, 10.1021/ac4042075, 2014.
Freedman, M. A.: Phase separation in organic aerosol, Chemical Society Reviews, 46, 7694-7705, 2017.
Fu, P., Kawamura, K., Chen, J., and Barrie, L. A.: Isoprene, monoterpene, and sesquiterpene oxidation products in the high Arctic aerosols during late winter to early summer, Environmental Science & Technology, 43, 4022-4028, 2009.
Fu, P. Q., Kawamura, K., Cheng, Y. F., Hatakeyama, S., Takami, A., Li, H., and Wang, W.: Aircraft measurements of polar organic tracer compounds in tropospheric particles (PM₁₀) over central China, Atmospheric Chemistry and Physics, 14, 4185-4199, 10.5194/acp-14-4185-2014, 2014.
Ge, Z., Wexler, A. S., and Johnston, M. V.: Multicomponent aerosol crystallization, Journal of Colloid and Interface Science, 183, 68-77, 1996.

693 Gibson, E. R., Hudson, P. K., and Grassian, V. H.: Physicochemical properties of nitrate aerosols:
694 Implications for the atmosphere, The Journal of Physical Chemistry A, 110, 11785-11799, 2006.
695 Gómez-González, Y., Wang, W., Vermeylen, R., Chi, X., Neirynck, J., Janssens, I. A., Maenhaut, W.,
696 and Claeys, M.: Chemical characterisation of atmospheric aerosols during a 2007 summer field
697 campaign at Brasschaat, Belgium: sources and source processes of biogenic secondary organic
698 aerosol, Atmospheric Chemistry and Physics, 12, 125-138, 10.5194/acp-12-125-2012, 2012.
699 Guenther, A., Hewitt, C. N., Erickson, D., Fall, R., Geron, C., Graedel, T., Harley, P., Klinger, L., Lerdau,
700 M., and McKay, W.: A global model of natural volatile organic compound emissions, Journal of
701 Geophysical Research: Atmospheres, 100, 8873-8892, 1995.
702 Gupta, D., Eom, H. J., Cho, H. R., and Ro, C. U.: Hygroscopic behavior of NaCl–MgCl2 mixture particles
703 as nascent sea-spray aerosol surrogates and observation of efflorescence during humidification,
704 Atmospheric Chemistry and Physics, 15, 11273-11290, 10.5194/acp-15-11273-2015, 2015.
705 Gysel, M., Weingartner, E., and Baltensperger, U.: Hygroscopicity of aerosol particles at low
706 temperatures. 2. Theoretical and experimental hygroscopic properties of laboratory generated
707 aerosols, Environmental science & technology, 36, 63-68, 2002.
708 Hallquist, M., Wenger, J. C., Baltensperger, U., Rudich, Y., Simpson, D., Claeys, M., Dommen, J.,
709 Donahue, N., George, C., and Goldstein, A.: The formation, properties and impact of secondary
710 organic aerosol: current and emerging issues, Atmospheric chemistry and physics, 9, 5155-5236,
711 2009.
712 Harris, D. C.: Exploring chemical analysis, Macmillan, 2012.
713 Haywood, J., and Boucher, O.: Estimates of the direct and indirect radiative forcing due to tropospheric
714 aerosols: A review, Reviews of geophysics, 38, 513-543, 2000.
715 Hoffman, R. C., Laskin, A., and Finlayson-Pitts, B. J.: Sodium nitrate particles: physical and chemical
716 properties during hydration and dehydration, and implications for aged sea salt aerosols, Journal
717 of Aerosol Science, 35, 869-887, 10.1016/j.jaerosci.2004.02.003, 2004.
718 Holopainen, J. K., Kivimaenpaa, M., and Nizkorodov, S. A.: Plant-derived Secondary Organic Material
719 in the Air and Ecosystems, Trends Plant Sci, 22, 744-753, 10.1016/j.tplants.2017.07.004, 2017.
720 Hong, Z., Zhang, H., Zhang, Y., Xu, L., Liu, T., Xiao, H., Hong, Y., Chen, J., Li, M., Deng, J., Wu, X.,
721 Hu, B., and Chen, X.: Secondary organic aerosol of PM2.5 in a mountainous forest area in
722 southeastern China: Molecular compositions and tracers implication, Sci Total Environ, 653, 496-
723 503, 10.1016/j.scitotenv.2018.10.370, 2019.
724 Hu, D., Bian, Q., Li, T. W. Y., Lau, A. K. H., and Yu, J. Z.: Contributions of isoprene, monoterpenes,β-
725 caryophyllene, and toluene to secondary organic aerosols in Hong Kong during the summer of
726 2006, Journal of Geophysical Research, 113, 10.1029/2008jd010437, 2008.
727 Hu, Q. H., Xie, Z. Q., Wang, X. M., Kang, H., He, Q. F., and Zhang, P.: Secondary organic aerosols over
728 oceans via oxidation of isoprene and monoterpenes from Arctic to Antarctic, Sci Rep, 3, 2280,
729 10.1038/srep02280, 2013.
730 Jang, M., Czoschke, N. M., Lee, S., and Kamens, R. M.: Heterogeneous atmospheric aerosol production
731 by acid-catalyzed particle-phase reactions, Science, 298, 814-817, 2002.
732 Jaoui, M., Kleindienst, T., Lewandowski, M., Offenberg, J., and Edney, E.: Identification and
733 quantification of aerosol polar oxygenated compounds bearing carboxylic or hydroxyl groups. 2.

734 Organic tracer compounds from monoterpenes, Environmental science & technology, 39, 5661-
735 5673, 2005.
736 Jimenez, J. L., Canagaratna, M., Donahue, N., Prevot, A., Zhang, Q., Kroll, J. H., DeCarlo, P. F., Allan,
737 J. D., Coe, H., and Ng, N.: Evolution of organic aerosols in the atmosphere, science, 326, 1525-
738 1529, 2009.
739 Jing, B., Tong, S., Liu, Q., Li, K., Wang, W., Zhang, Y., and Ge, M.: Hygroscopic behavior of
740 multicomponent organic aerosols and their internal mixtures with ammonium sulfate,
741 Atmospheric Chemistry and Physics, 16, 4101-4118, 10.5194/acp-16-4101-2016, 2016.
742 Jing, B., Wang, Z., Tan, F., Guo, Y., Tong, S., Wang, W., Zhang, Y., and Ge, M.: Hygroscopic behavior
743 of atmospheric aerosols containing nitrate salts and water-soluble organic acids, Atmospheric
744 Chemistry and Physics, 18, 5115-5127, 10.5194/acp-18-5115-2018, 2018.
745 Kammer, J., Perraudin, E., Flaud, P. M., Lamaud, E., Bonnefond, J. M., and Villenave, E.: Observation
746 of nighttime new particle formation over the French Landes forest, Sci Total Environ, 621, 1084-
747 1092, 10.1016/j.scitotenv.2017.10.118, 2018.
748 Kang, M., Fu, P., Kawamura, K., Yang, F., Zhang, H., Zang, Z., Ren, H., Ren, L., Zhao, Y., Sun, Y., and
749 Wang, Z.: Characterization of biogenic primary and secondary organic aerosols in the marine
750 atmosphere over the East China Sea, Atmospheric Chemistry and Physics, 18, 13947-13967,
751 10.5194/acp-18-13947-2018, 2018.
752 Karadima, K. S., Mavrantzas, V. G., and Pandis, S. N.: Insights into the morphology of multicomponent
753 organic and inorganic aerosols from molecular dynamics simulations, Atmospheric Chemistry and
754 Physics, 19, 5571-5587, 10.5194/acp-19-5571-2019, 2019.
755 Kerminen, V.-M., Pakkanen, T. A., and Hillamo, R. E.: Interactions between inorganic trace gases and
756 supermicrometer particles at a coastal site, Atmospheric Environment, 31, 2753-2765, 1997.
757 Kidd, C., Perraud, V., Wingen, L. M., and Finlayson-Pitts, B. J.: Integrating phase and composition of
758 secondary organic aerosol from the ozonolysis of α-pinene, Proceedings of the National Academy
759 of Sciences, 111, 7552-7557, 2014.
760 Kildgaard, J. V., Mikkelsen, K. V., Bilde, M., and Elm, J.: Hydration of Atmospheric Molecular Clusters
761 II: Organic Acid-Water Clusters, J Phys Chem A, 122, 8549-8556, 10.1021/acs.jpca.8b07713,
762 2018.
763 Kim, H., Lee, M.-J., Jung, H.-J., Eom, H.-J., Maskey, S., Ahn, K.-H., and Ro, C.-U.: Hygroscopic
764 behavior of wet dispersed and dry deposited NaNO3 particles, Atmospheric Environment, 60, 68-
765 75, 10.1016/j.atmosenv.2012.06.011, 2012.
766 Kim, H., Zhang, Q., and Heo, J.: Influence of intense secondary aerosol formation and long-range
767 transport on aerosol chemistry and properties in the Seoul Metropolitan Area during spring time:
768 results from KORUS-AQ, Atmospheric Chemistry and Physics, 18, 7149-7168, 10.5194/acp-18-
769 7149-2018, 2018.
770 Koop, T., Bookhold, J., Shiraiwa, M., and Pöschl, U.: Glass transition and phase state of organic
771 compounds: dependency on molecular properties and implications for secondary organic aerosols
772 in the atmosphere, Physical Chemistry Chemical Physics, 13, 19238-19255, 2011.
773 Kostenidou, E., Karnezi, E., Kolodziejczyk, A., Szmigielski, R., and Pandis, S. N.: Physical and Chemical
774 Properties of 3-Methyl-1,2,3-butanetricarboxylic Acid (MBTCA) Aerosol, Environ Sci Technol,
775 52, 1150-1155, 10.1021/acs.est.7b04348, 2018.

776 Kourtchev, I., Copolovici, L., Claeys, M., and Maenhaut, W.: Characterization of atmospheric aerosols
777 at a forested site in Central Europe, Environmental science & technology, 43, 4665-4671, 2009.
778 Kroll, J. H., and Seinfeld, J. H.: Chemistry of secondary organic aerosol: Formation and evolution of low-
779 volatility organics in the atmosphere, Atmospheric Environment, 42, 3593-3624, 2008.
780 Kubátová, A., Vermeylen, R., Claeys, M., Cafmeyer, J., Maenhaut, W., Roberts, G., and Artaxo, P.:
781 Carbonaceous aerosol characterization in the Amazon basin, Brazil: novel dicarboxylic acids and
782 related compounds, Atmospheric Environment, 34, 5037-5051, 2000.
783 Kubátová, A., Vermeylen, R., Claeys, M., Cafmeyer, J., and Maenhaut, W.: Organic compounds in urban
784 aerosols from Gent, Belgium: Characterization, sources, and seasonal differences, Journal of
785 Geophysical Research: Atmospheres, 107, ICC 5-1-ICC 5-12, 10.1029/2001jd000556, 2002.
786 Lai, C., Liu, Y., Ma, J., Ma, Q., Chu, B., and He, H.: Heterogeneous Kinetics of cis-Pinonic Acid with
787 Hydroxyl Radical under Different Environmental Conditions, J Phys Chem A, 119, 6583-6593,
788 10.1021/acs.jpca.5b01321, 2015.
789 Laskin, A., Moffet, R. C., Gilles, M. K., Fast, J. D., Zaveri, R. A., Wang, B., Nigge, P., and Shutthanandan,
790 J.: Tropospheric chemistry of internally mixed sea salt and organic particles: Surprising reactivity
791 of NaCl with weak organic acids, Journal of Geophysical Research: Atmospheres, 117, n/a-n/a,
792 10.1029/2012jd017743, 2012.
793 Lee, A. K. Y., Ling, T. Y., and Chan, C. K.: Understanding hygroscopic growth and phase transformation
794 of aerosols using single particle Raman spectroscopy in an electrodynamic balance, Faraday
795 Discuss., 137, 245-263, 10.1039/b704580h, 2008.
796 Lessmeier, J., Dette, H. P., Godt, A., and Koop, T.: Physical state of 2-methylbutane-1,2,3,4-tetraol in
797 pure and internally mixed aerosols, Atmospheric Chemistry and Physics, 18, 15841-15857,
798 10.5194/acp-18-15841-2018, 2018.
799 Li, J. J., Wang, G. H., Cao, J. J., Wang, X. M., and Zhang, R. J.: Observation of biogenic secondary
800 organic aerosols in the atmosphere of a mountain site in central China: temperature and relative
801 humidity effects, Atmospheric Chemistry and Physics, 13, 11535-11549, 10.5194/acp-13-11535-
802 2013, 2013.
803 Li, X., Gupta, D., Eom, H.-J., Kim, H., and Ro, C.-U.: Deliquescence and efflorescence behavior of
804 individual NaCl and KCl mixture aerosol particles, Atmospheric Environment, 82, 36-43,
805 10.1016/j.atmosenv.2013.10.011, 2014.
806 Li, X., Gupta, D., Lee, J., Park, G., and Ro, C. U.: Real-Time Investigation of Chemical Compositions
807 and Hygroscopic Properties of Aerosols Generated from NaCl and Malonic Acid Mixture
808 Solutions Using in Situ Raman Microspectrometry, Environ Sci Technol, 51, 263-270,
809 10.1021/acs.est.6b04356, 2017.
810 Li, X., Song, S., Zhou, W., Hao, J., Worsnop, D. R., and Jiang, J.: Interactions between aerosol organic
811 components and liquid water content during haze episodes in Beijing, Atmospheric Chemistry and
812 Physics, 19, 12163-12174, 10.5194/acp-19-12163-2019, 2019.
813 Lightstone, J. M., Onasch, T. B., Imre, D., and Oatis, S.: Deliquescence, efflorescence, and water activity
814 in ammonium nitrate and mixed ammonium nitrate/succinic acid microparticles, The Journal of
815 Physical Chemistry A, 104, 9337-9346, 2000.

Lignell, H., Epstein, S. A., Marvin, M. R., Shemesh, D., Gerber, B., and Nizkorodov, S.: Experimental and theoretical study of aqueous cis-pinonic acid photolysis, J Phys Chem A, 117, 12930-12945, 10.1021/jp4093018, 2013.

Liu, T., Zhou, L., Liu, Q., Lee, B. P., Yao, D., Lu, H., Lyu, X., Guo, H., and Chan, C. K.: Secondary Organic Aerosol Formation from Urban Roadside Air in Hong Kong, Environ Sci Technol, 53, 3001-3009, 10.1021/acs.est.8b06587, 2019.

Ma, Q., Ma, J., Liu, C., Lai, C., and He, H.: Laboratory study on the hygroscopic behavior of external and internal C2-C4 dicarboxylic acid-NaCl mixtures, Environ Sci Technol, 47, 10381-10388, 10.1021/es4023267, 2013.

Marsh, A., Rovelli, G., Miles, R. E. H., and Reid, J. P.: Complexity of Measuring and Representing the Hygroscopicity of Mixed Component Aerosol, J Phys Chem A, 123, 1648-1660, 10.1021/acs.jpca.8b11623, 2019.

Martin, S. T.: Phase transitions of aqueous atmospheric particles, Chemical Reviews, 100, 3403-3454, 2000.

Mikhailov, E., Vlasenko, S., Martin, S., Koop, T., and Pöschl, U.: Amorphous and crystalline aerosol particles interacting with water vapor: conceptual framework and experimental evidence for restructuring, phase transitions and kinetic limitations, Atmospheric Chemistry and Physics, 9, 9491-9522, 2009.

Miyazaki, Y., Jung, J., Fu, P., Mizoguchi, Y., Yamanoi, K., and Kawamura, K.: Evidence of formation of submicrometer water-soluble organic aerosols at a deciduous forest site in northern Japan in summer, Journal of Geophysical Research: Atmospheres, 117, n/a-n/a, 10.1029/2012jd018250, 2012.

Müller, L., Reinnig, M. C., Naumann, K. H., Saathoff, H., Mentel, T. F., Donahue, N. M., and Hoffmann, T.: Formation of 3-methyl-1,2,3-butanetricarboxylic acid via gas phase oxidation of pinonic acid – a mass spectrometric study of SOA aging, Atmospheric Chemistry and Physics, 12, 1483-1496, 10.5194/acp-12-1483-2012, 2012.

Mutzel, A., Rodigast, M., Iinuma, Y., Böge, O., and Herrmann, H.: Monoterpene SOA–contribution of first-generation oxidation products to formation and chemical composition, Atmospheric environment, 130, 136-144, 2016.

Pajunoja, A., Hu, W., Leong, Y. J., Taylor, N. F., Miettinen, P., Palm, B. B., Mikkonen, S., Collins, D. R., Jimenez, J. L., and Virtanen, A.: Phase state of ambient aerosol linked with water uptake and chemical aging in the southeastern US, Atmospheric Chemistry and Physics, 16, 11163-11176, 2016.

Parsons, M. T., Knopf, D. A., and Bertram, A. K.: Deliquescence and Crystallization of Ammonium Sulfate Particles Internally Mixed with Water-Soluble Organic Compounds, The Journal of Physical Chemistry A, 108, 11600-11608, 10.1021/jp0462862, 2004.

Pöhlker, C., Saturno, J., Krüger, M. L., Förster, J.-D., Weigand, M., Wiedemann, K. T., Bechtel, M., Artaxo, P., and Andreae, M. O.: Efflorescence upon humidification? X-ray microspectroscopic in situ observation of changes in aerosol microstructure and phase state upon hydration, Geophysical Research Letters, 41, 3681-3689, 10.1002/2014gl059409, 2014.

856 Poschl, U., and Shiraiwa, M.: Multiphase chemistry at the atmosphere-biosphere interface influencing
857 climate and public health in the anthropocene, Chem Rev, 115, 4440-4475, 10.1021/cr500487s,
858 2015.
859 Praplan, A. P., Barmet, P., Dommen, J., and Baltensperger, U.: Cyclobutyl methyl ketone as a model
860 compound for pinonic acid to elucidate oxidation mechanisms, Atmospheric Chemistry and
861 Physics, 12, 10749-10758, 10.5194/acp-12-10749-2012, 2012.
862 Reid, J. P., Bertram, A. K., Topping, D. O., Laskin, A., Martin, S. T., Petters, M. D., Pope, F. D., and
863 Rovelli, G.: The viscosity of atmospherically relevant organic particles, Nat Commun, 9, 956,
864 10.1038/s41467-018-03027-z, 2018.
865 Renbaum-Wolff, L., Grayson, J. W., Bateman, A. P., Kuwata, M., Sellier, M., Murray, B. J., Shilling, J.
866 E., Martin, S. T., and Bertram, A. K.: Viscosity of alpha-pinene secondary organic material and
867 implications for particle growth and reactivity, Proc Natl Acad Sci U S A, 110, 8014-8019,
868 10.1073/pnas.1219548110, 2013.
869 Rudich, Y., Donahue, N. M., and Mentel, T. F.: Aging of organic aerosol: Bridging the gap between
870 laboratory and field studies, Annual Review of Physical Chemistry, 58, 321-352,
871 10.1146/annurev.physchem.58.032806.104432, 2007.
872 Sato, K., Jia, T., Tanabe, K., Morino, Y., Kajii, Y., and Imamura, T.: Terpenylic acid and nine-carbon
873 multifunctional compounds formed during the aging of β-pinene ozonolysis secondary organic
874 aerosol, Atmospheric Environment, 130, 127-135, 10.1016/j.atmosenv.2015.08.047, 2016.
875 Saukko, E., Lambe, A. T., Massoli, P., Koop, T., Wright, J. P., Croasdale, D. R., Pedernera, D. A., Onasch,
876 T. B., Laaksonen, A., Davidovits, P., Worsnop, D. R., and Virtanen, A.: Humidity-dependent
877 phase state of SOA particles from biogenic and anthropogenic precursors, Atmospheric Chemistry
878 and Physics, 12, 7517-7529, 10.5194/acp-12-7517-2012, 2012.
879 Schlenker, J. C., and Martin, S. T.: Crystallization pathways of sulfate− nitrate− ammonium aerosol
880 particles, The Journal of Physical Chemistry A, 109, 9980-9985, 2005.
881 Seaver, M., Galloway, A., and Manuccia, T. J.: Acoustic levitation in a free-jet wind tunnel, Review of
882 Scientific Instruments, 60, 3452-3459, 10.1063/1.1140492, 1989.
883 Seng, S., Guo, F., Tobon, Y. A., Ishikawa, T., Moreau, M., Ishizaka, S., and Sobanska, S.: Deliquescence
884 behavior of photo-irradiated single NaNO3 droplets, Atmospheric Environment, 183, 33-39,
885 10.1016/j.atmosenv.2018.04.007, 2018.
886 Shiraiwa, M., Li, Y., Tsimpidi, A. P., Karydis, V. A., Berkemeier, T., Pandis, S. N., Lelieveld, J., Koop,
887 T., and Poschl, U.: Global distribution of particle phase state in atmospheric secondary organic
888 aerosols, Nat Commun, 8, 15002, 10.1038/ncomms15002, 2017.
889 Shrivastava, M., Easter, R. C., Liu, X., Zelenyuk, A., Singh, B., Zhang, K., Ma, P.-L., Chand, D., Ghan,
890 S., Jimenez, J. L., Zhang, Q., Fast, J., Rasch, P. J., and Tiitta, P.: Global transformation and fate
891 of SOA: Implications of low-volatility SOA and gas-phase fragmentation reactions, Journal of
892 Geophysical Research: Atmospheres, 120, 4169-4195, 10.1002/2014jd022563, 2015.
893 Shrivastava, M., Cappa, C. D., Fan, J., Goldstein, A. H., Guenther, A. B., Jimenez, J. L., Kuang, C.,
894 Laskin, A., Martin, S. T., Ng, N. L., Petaja, T., Pierce, J. R., Rasch, P. J., Roldin, P., Seinfeld, J.
895 H., Shilling, J., Smith, J. N., Thornton, J. A., Volkamer, R., Wang, J., Worsnop, D. R., Zaveri, R.
896 A., Zelenyuk, A., and Zhang, Q.: Recent advances in understanding secondary organic aerosol:

Implications for global climate forcing, Reviews of Geophysics, 55, 509-559, 10.1002/2016rg000540, 2017.
Slade, J. H., Ault, A. P., Bui, A. T., Ditto, J. C., Lei, Z., Bondy, A. L., Olson, N. E., Cook, R. D., Desrochers, S. J., Harvey, R. M., Erickson, M. H., Wallace, H. W., Alvarez, S. L., Flynn, J. H., Boor, B. E., Petrucci, G. A., Gentner, D. R., Griffin, R. J., and Shepson, P. B.: Bouncier Particles at Night: Biogenic Secondary Organic Aerosol Chemistry and Sulfate Drive Diel Variations in the Aerosol Phase in a Mixed Forest, Environ Sci Technol, 53, 4977-4987, 10.1021/acs.est.8b07319, 2019.
Song, M., Maclean, A. M., Huang, Y., Smith, N. R., Blair, S. L., Laskin, J., Laskin, A., DeRieux, W.-S. W., Li, Y., Shiraiwa, M., Nizkorodov, S. A., and Bertram, A. K.: Liquid–liquid phase separation and viscosity within secondary organic aerosol generated from diesel fuel vapors, Atmospheric Chemistry and Physics, 19, 12515-12529, 10.5194/acp-19-12515-2019, 2019.
Song, Y. C., Haddrell, A. E., Bzdek, B. R., Reid, J. P., Bannan, T., Topping, D. O., Percival, C., and Cai, C.: Measurements and predictions of binary component aerosol particle viscosity, The Journal of Physical Chemistry A, 120, 8123-8137, 2016.
Srivastava, D., Favez, O., Perraudin, E., Villenave, E., and Albinet, A.: Comparison of Measurement-Based Methodologies to Apportion Secondary Organic Carbon (SOC) in PM2.5: A Review of Recent Studies, Atmosphere, 9, 10.3390/atmos9110452, 2018.
Sun, J., Liu, L., Xu, L., Wang, Y., Wu, Z., Hu, M., Shi, Z., Li, Y., Zhang, X., Chen, J., and Li, W.: Key Role of Nitrate in Phase Transitions of Urban Particles: Implications of Important Reactive Surfaces for Secondary Aerosol Formation, Journal of Geophysical Research: Atmospheres, 123, 1234-1243, 10.1002/2017jd027264, 2018.
Szmigielski, R., Surratt, J. D., Gómez-González, Y., Van der Veken, P., Kourtchev, I., Vermeylen, R., Blockhuys, F., Jaoui, M., Kleindienst, T. E., Lewandowski, M., Offenberg, J. H., Edney, E. O., Seinfeld, J. H., Maenhaut, W., and Claeys, M.: 3-methyl-1,2,3-butanetricarboxylic acid: An atmospheric tracer for terpene secondary organic aerosol, Geophysical Research Letters, 34, 10.1029/2007gl031338, 2007.
Tang, M., Chan, C. K., Li, Y. J., Su, H., Ma, Q., Wu, Z., Zhang, G., Wang, Z., Ge, M., Hu, M., He, H., and Wang, X.: A review of experimental techniques for aerosol hygroscopicity studies, Atmospheric Chemistry and Physics, 19, 12631-12686, 10.5194/acp-19-12631-2019, 2019.
Topping, D., Connolly, P., and McFiggans, G.: Cloud droplet number enhanced by co-condensation of organic vapours, Nature Geoscience, 6, 443, 2013.
Virtanen, A., Joutsensaari, J., Koop, T., Kannosto, J., Yli-Pirilä, P., Leskinen, J., Mäkelä, J. M., Holopainen, J. K., Pöschl, U., and Kulmala, M.: An amorphous solid state of biogenic secondary organic aerosol particles, Nature, 467, 824, 2010.
Vlachou, A., Tobler, A., Lamkaddam, H., Canonaco, F., Daellenbach, K. R., Jaffrezo, J.-L., Minguillón, M. C., Maasikmets, M., Teinemaa, E., Baltensperger, U., El Haddad, I., and Prévôt, A. S. H.: Development of a versatile source apportionment analysis based on positive matrix factorization: a case study of the seasonal variation of organic aerosol sources in Estonia, Atmospheric Chemistry and Physics, 19, 7279-7295, 10.5194/acp-19-7279-2019, 2019.
Vogel, A. L., Äijälä, M., Corrigan, A. L., Junninen, H., Ehn, M., Petäjä, T., Worsnop, D. R., Kulmala, M., Russell, L. M., Williams, J., and Hoffmann, T.: In situ submicron organic aerosol

characterization at a boreal forest research station during HUMPPA-COPEC 2010 using soft and hard ionization mass spectrometry, Atmospheric Chemistry and Physics, 13, 10933-10950, 10.5194/acp-13-10933-2013, 2013.

Wang, B., O'Brien, R. E., Kelly, S. T., Shilling, J. E., Moffet, R. C., Gilles, M. K., and Laskin, A.: Reactivity of liquid and semisolid secondary organic carbon with chloride and nitrate in atmospheric aerosols, J Phys Chem A, 119, 4498-4508, 10.1021/jp510336q, 2015.

Wang, X., Jing, B., Tan, F., Ma, J., Zhang, Y., and Ge, M.: Hygroscopic behavior and chemical composition evolution of internally mixed aerosols composed of oxalic acid and ammonium sulfate, Atmospheric Chemistry and Physics, 17, 12797-12812, 10.5194/acp-17-12797-2017, 2017.

Wang, Z., Jing, B., Shi, X., Tong, S., Wang, W., and Ge, M.: Importance of water-soluble organic acid on the hygroscopicity of nitrate, Atmospheric Environment, 190, 65-73, 10.1016/j.atmosenv.2018.07.010, 2018.

Wu, L., Li, X., Kim, H., Geng, H., Godoi, R. H. M., Barbosa, C. G. G., Godoi, A. F. L., Yamamoto, C. I., de Souza, R. A. F., Pöhlker, C., Andreae, M. O., and Ro, C.-U.: Single-particle characterization of aerosols collected at a remote site in the Amazonian rainforest and an urban site in Manaus, Brazil, Atmospheric Chemistry and Physics, 19, 1221-1240, 10.5194/acp-19-1221-2019, 2019a.

Wu, L., Li, X., and Ro, C.-U.: Hygroscopic Behavior of Ammonium Sulfate, Ammonium Nitrate, and their Mixture Particles, Asian Journal of Atmospheric Environment, 13, 196-211, 10.5572/ajae.2019.13.3.196, 2019b.

Wu, L., and Ro, C.-U.: Aerosol Hygroscopicity on A Single Particle Level Using Microscopic and Spectroscopic Techniques: A Review, Asian Journal of Atmospheric Environment, 14, 177-209, 10.5572/ajae.2020.14.3.177, 2020.

Wu, Z. J., Nowak, A., Poulain, L., Herrmann, H., and Wiedensohler, A.: Hygroscopic behavior of atmospherically relevant water-soluble carboxylic salts and their influence on the water uptake of ammonium sulfate, Atmospheric Chemistry and Physics, 11, 12617-12626, 10.5194/acp-11-12617-2011, 2011.

Yasmeen, F., Szmigielski, R., Vermeylen, R., Gomez-Gonzalez, Y., Surratt, J. D., Chan, A. W., Seinfeld, J. H., Maenhaut, W., and Claeys, M.: Mass spectrometric characterization of isomeric terpenoic acids from the oxidation of alpha-pinene, beta-pinene, d-limonene, and Delta3-carene in fine forest aerosol, J Mass Spectrom, 46, 425-442, 10.1002/jms.1911, 2011.

Yatavelli, R. L. N., Mohr, C., Stark, H., Day, D. A., Thompson, S. L., Lopez-Hilfiker, F. D., Campuzano-Jost, P., Palm, B. B., Vogel, A. L., Hoffmann, T., Heikkinen, L., Äijälä, M., Ng, N. L., Kimmel, J. R., Canagaratna, M. R., Ehn, M., Junninen, H., Cubison, M. J., Petäjä, T., Kulmala, M., Jayne, J. T., Worsnop, D. R., and Jimenez, J. L.: Estimating the contribution of organic acids to northern hemispheric continental organic aerosol, Geophysical Research Letters, 42, 6084-6090, 10.1002/2015gl064650, 2015.

Zhang, Y. Y., Müller, L., Winterhalter, R., Moortgat, G. K., Hoffmann, T., and Pöschl, U.: Seasonal cycle and temperature dependence of pinene oxidation products, dicarboxylic acids and nitrophenols in fine and coarse air particulate matter, Atmospheric Chemistry and Physics, 10, 7859-7873, 10.5194/acp-10-7859-2010, 2010.

Figure 1. Calculated titration curve for MBTCA, noted as H_3M in this figure. The experimental data are shown as orange triangles. 5 mL of 0.02 M H_3M was titrated with a 0.1 M NaOH solution.

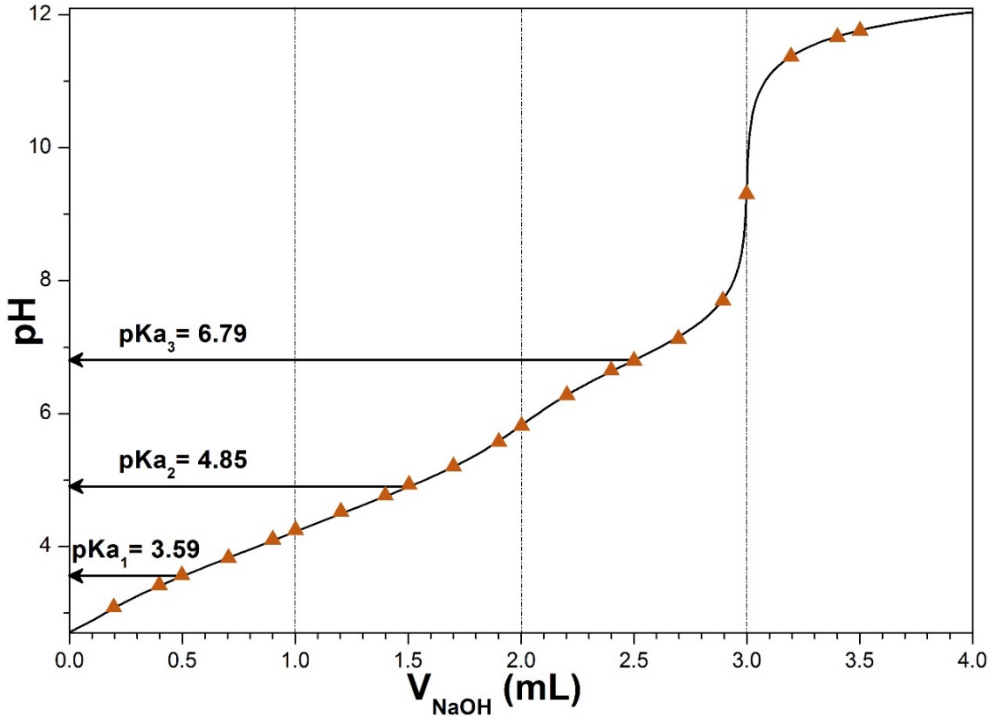

Figure 2. Hygroscopic curves, corresponding optical images, and Raman spectra at specific RHs of three types of pure MBTCA particles. The transition RHs recorded during the dehydration (D) and humidification (H) processes are marked with arrows in the hygroscopic curves.

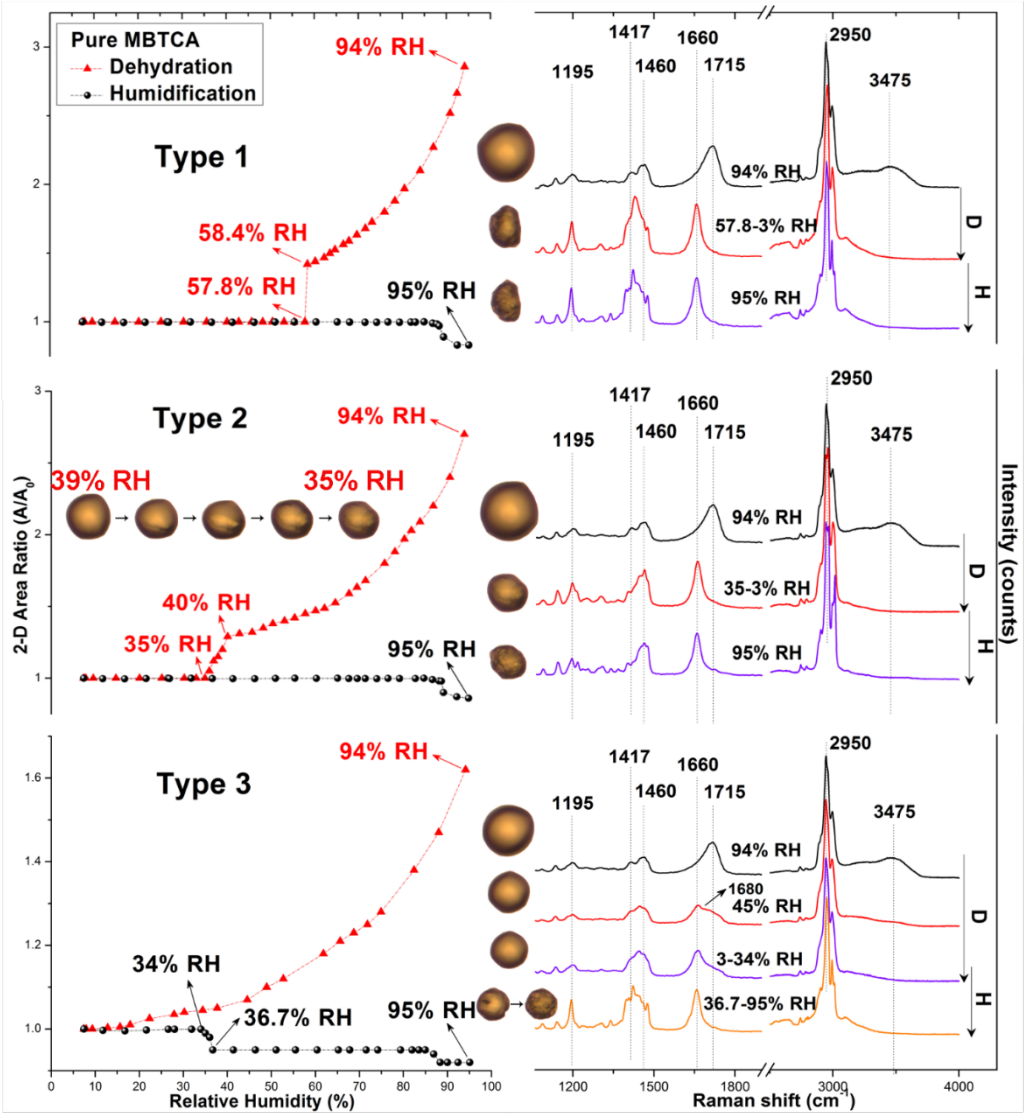

Figure 3. Hygroscopic curves, corresponding optical images, and Raman spectra at specific RHs of (a) mono-, (b) di-, and (c) tri-sodium MBTCA salt aerosols. The recorded transition RHs during the dehydration and humidification processes are marked with arrows in the hygroscopic curves.

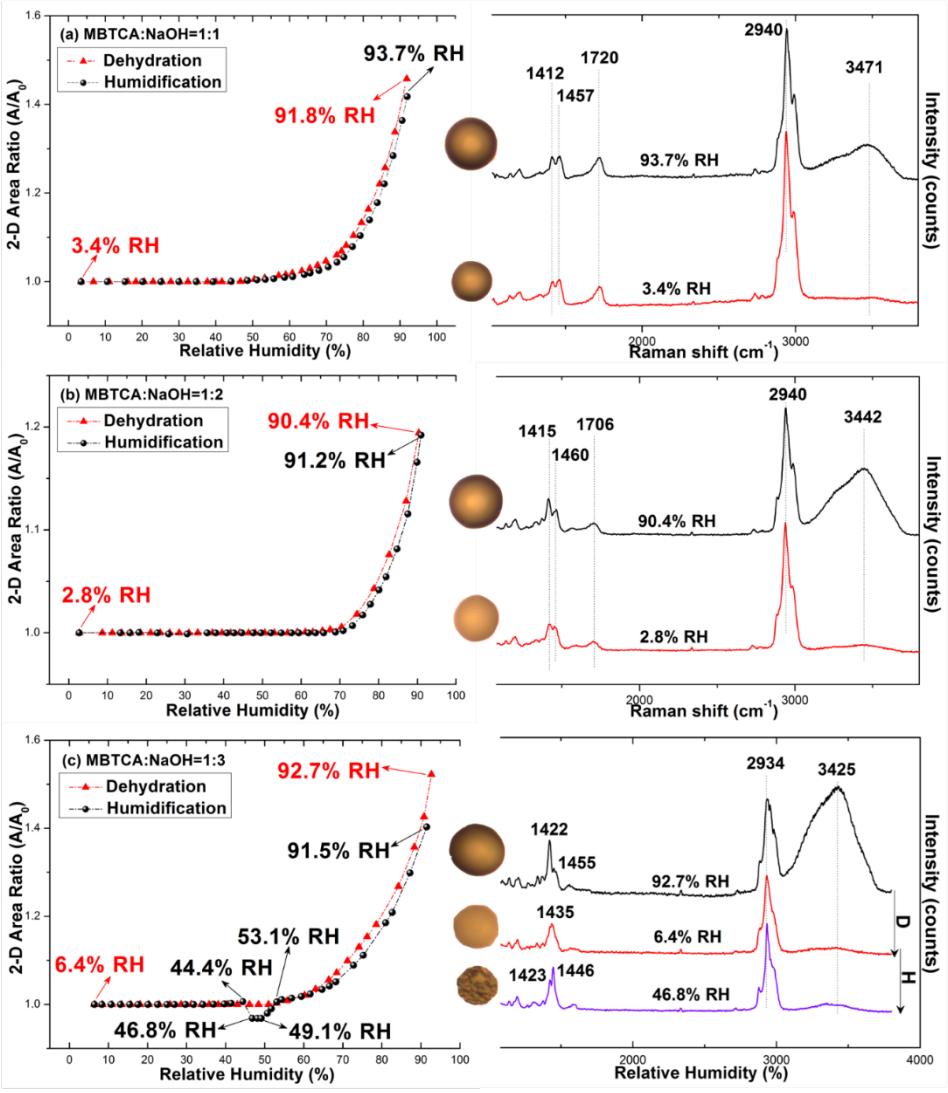

Figure 4. Hygroscopic curves, corresponding optical images, and Raman spectra at specific RHs of MBTCA:NaCl = (a) 1:1 and (b) 2:1. The recorded transition RHs during the dehydration (D) and humidification (H) processes and the chemical compositions of the mixtures at certain RHs are marked with arrows in the hygroscopic curves. The phase notations shown in parenthesis are s=solid; aq=aqueous; and as=amorphous solid.

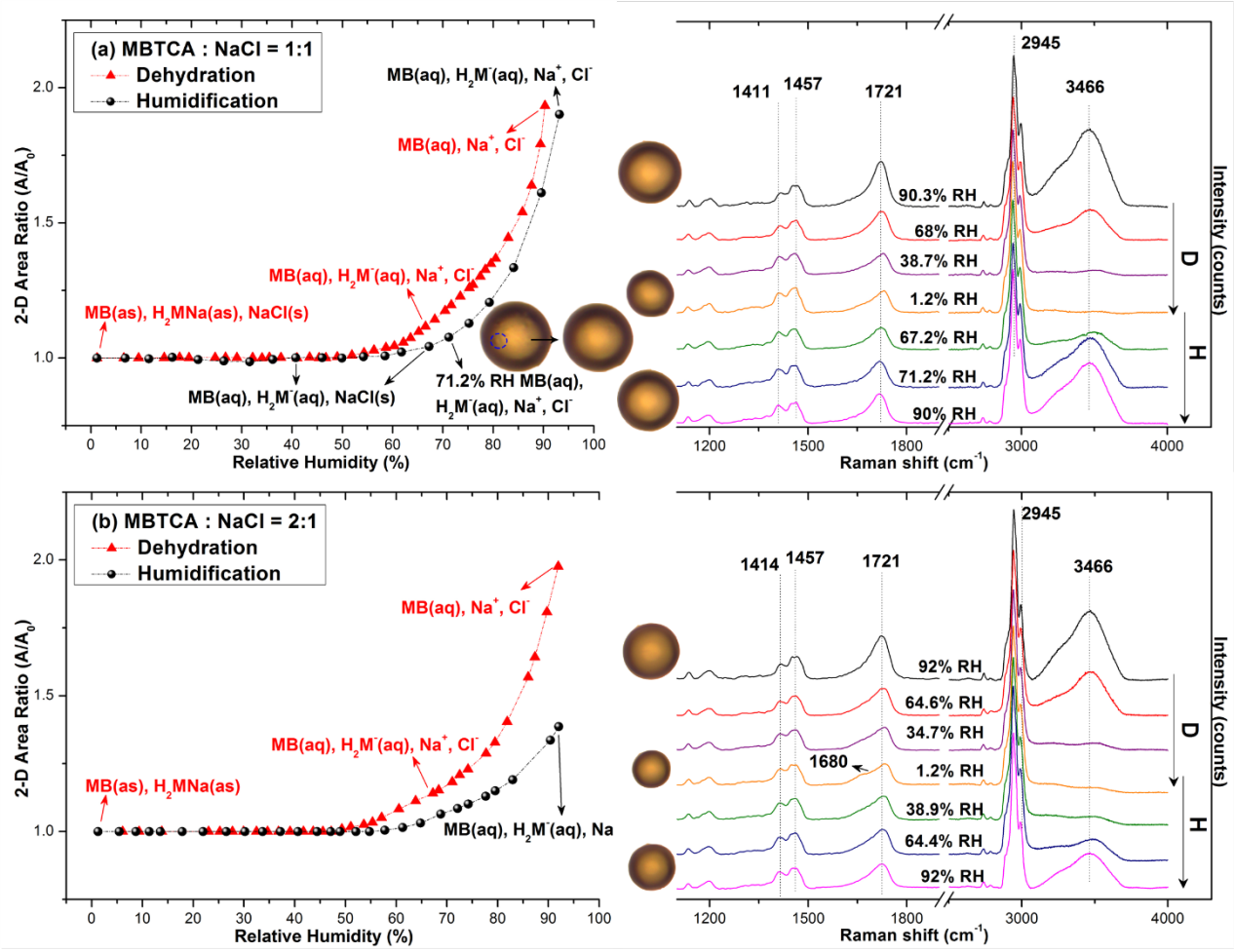

Figure 5. Hygroscopic curves, corresponding optical images, and Raman spectra at specific RHs of MBTCA:NaCl = (a) 1:2 and (b) 1:3. The recorded transition RHs during the dehydration (D) and humidification (H) processes and the chemical compositions of the mixtures at certain RHs are marked with arrows in the hygroscopic curves. The phase notations shown in parenthesis are s=solid; aq=aqueous; and as=amorphous solid.

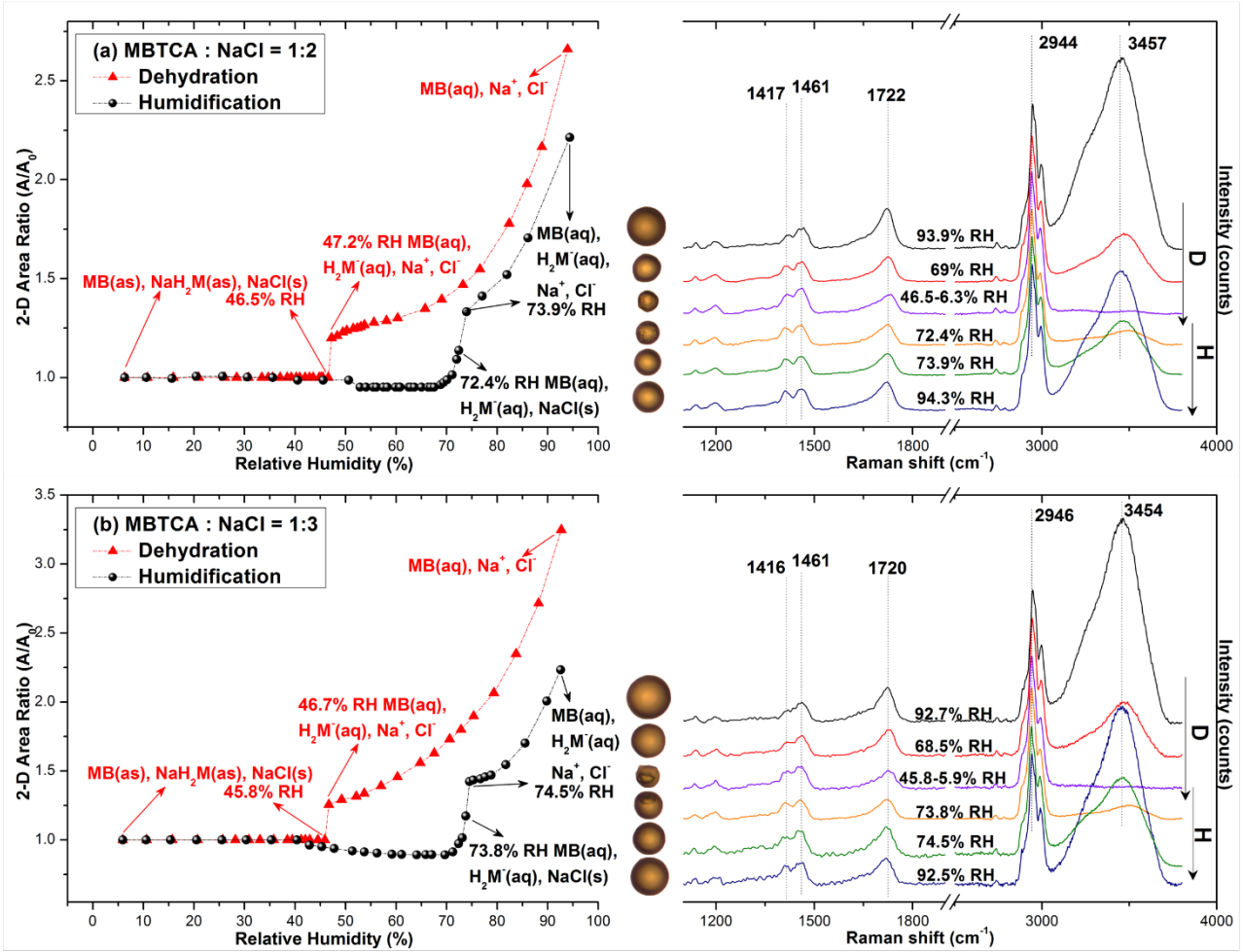

Figure 6. (a) Raman spectra of pure NaH_2M and mixture aerosols with mixing ratios of MBTCA:NaCl = 1:1, 1:2, and 1:3 obtained at the end of the humidification process, which were normalized to the CH_3 peak at 1458 cm^{-1} and (b) Raman spectra of pure MBTCA, mixture of MBTCA:NaH_2M = 1:1, and pure NaH_2M, which are normalized to the CH_3 peak at 1460 cm^{-1}.

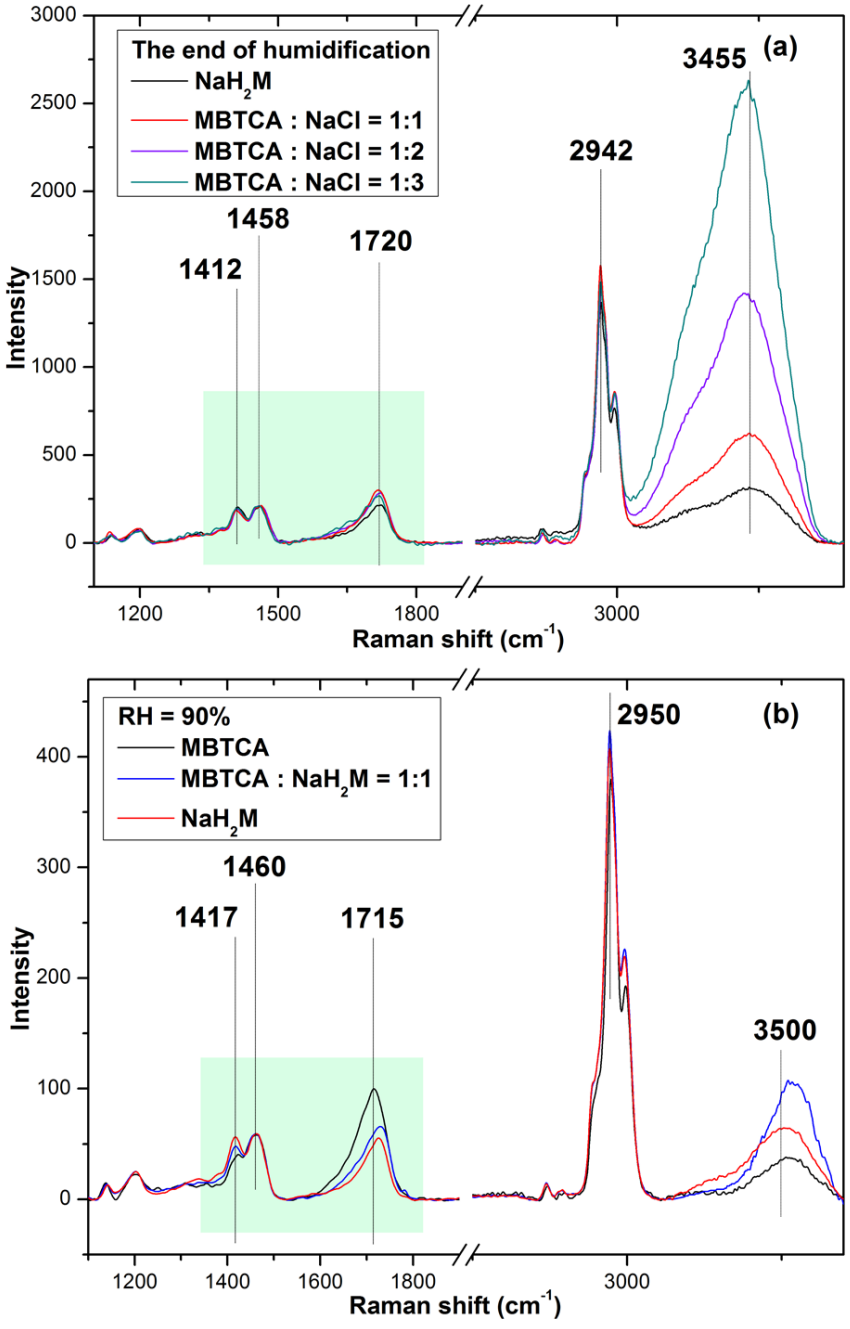

Figure 7. (a) Calibration curve calculated from the intensity ratios of two peaks at 1460 and 1720 cm^{-1} as a function of RH for NaH_2M, MBTCA:NaH_2M = 1:1, and MBTCA aerosols; (b) chemical reactivity represented as the degree of reaction for mixture aerosols of MBTCA:NaCl = 1:1, 1:2, 1:3, and 2:1 during the dehydration and humidification processes.

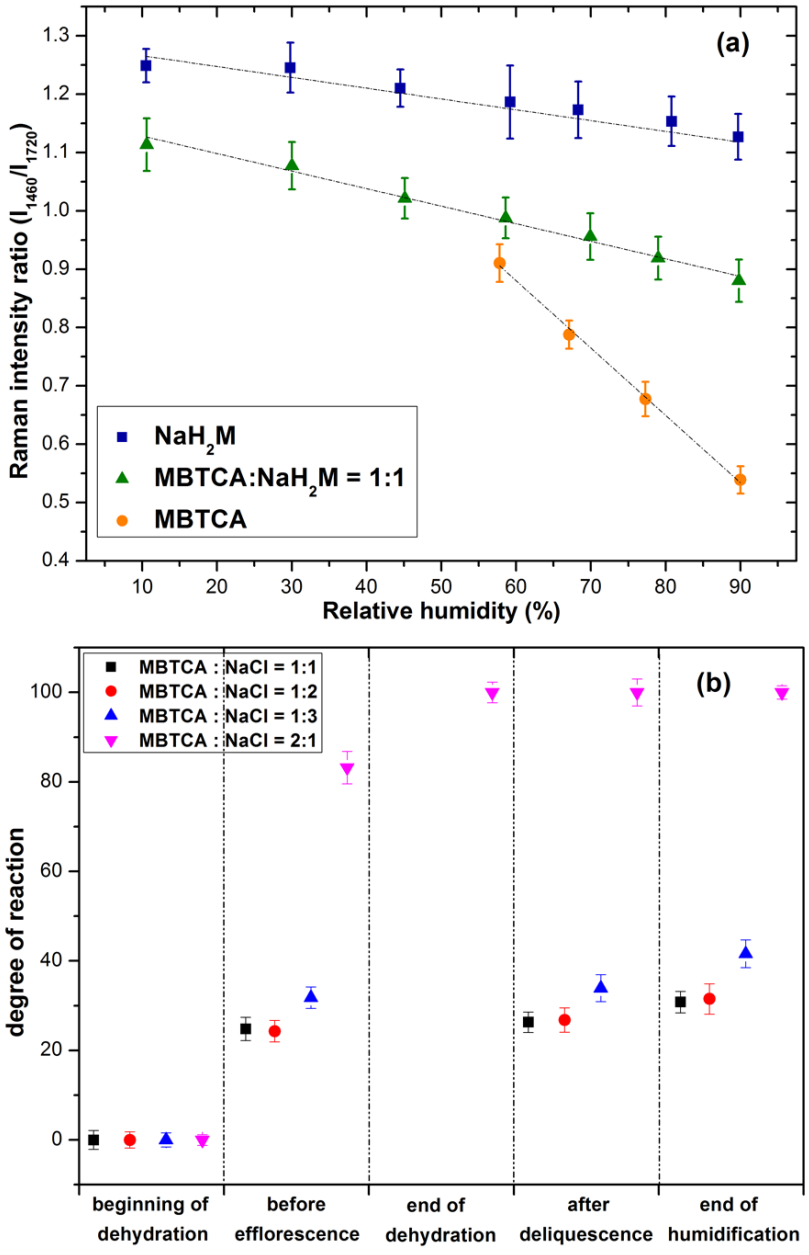

Figure 8. (a) Secondary electron images (SEIs) and elemental X-ray maps for C (from MBTCA and NaH_2M), Na (from NaH_2M and NaCl), and Cl (from NaCl). The scale bars are for 5 μm; (b) X-ray spectra and elemental concentrations of particles with four mixing ratios.

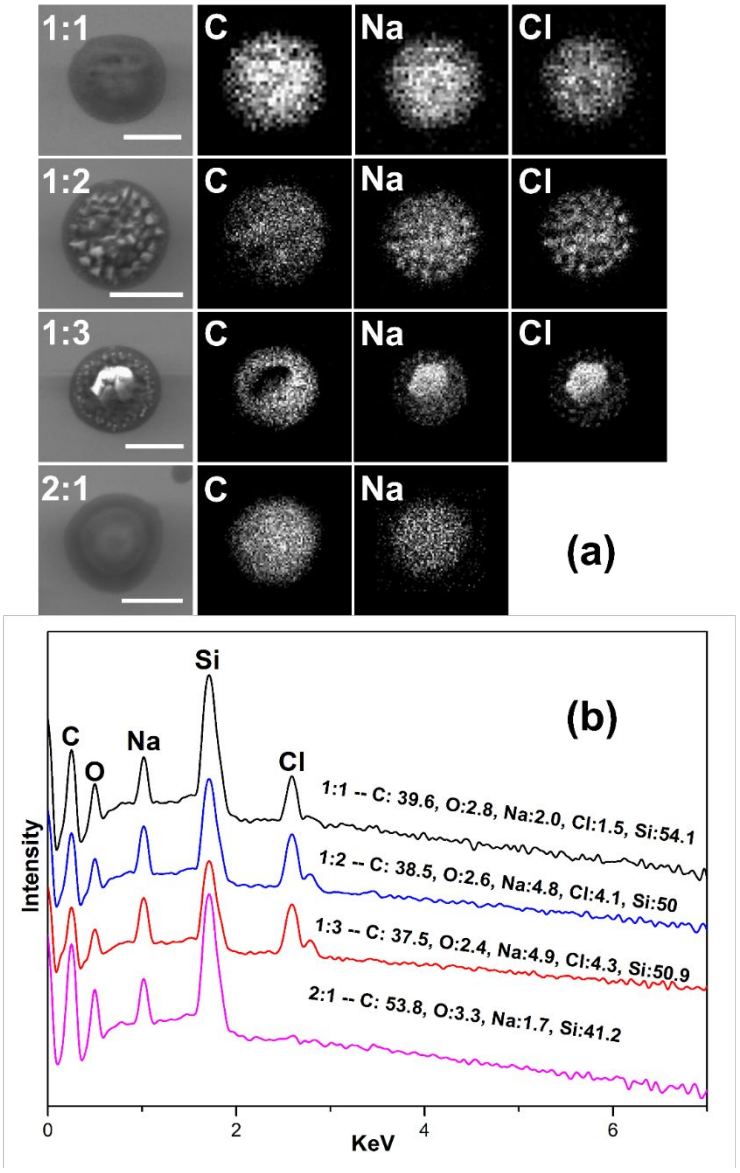

Figure 9. Hygroscopic curves, corresponding optical images, and Raman spectra at specific RHs of MBTCA:NaCl = (a) 1:1, (b) 1:2, and (c) 1:3 mixture particles in the levitation system. The recorded transition RHs during the humidification (H) and dehydration (D) processes and the chemical compositions of the mixtures at certain RHs are marked with arrows in the hygroscopic curves. The phase notations shown in parenthesis are s=solid; aq=aqueous; and as=amorphous solid.